

DiscoTEX 1.0: Discontinuous collocation and implicit-turned-explicit (IMTEX) integration symplectic, symmetric numerical algorithms with high order jumps for differential equations II: time-integration extension to higher-orders of numerical convergence

Lidia J. Gomes Da Silva

^a*School of Mathematical Sciences, Queen Mary University of London, London, E1 4NS, UK*

Abstract

DiscoTEX is a highly accurate numerical algorithm for computing numerical weak-form solutions to distributionally sourced partial differential equations (PDE)s. The aim of this second paper, succeeding [1], is to present its extension up to twelve orders. This will be demonstrated by computing numerical weak-form solutions to the distributionally sourced wave equation and comparing it to its exact solutions. The full details of the numerical scheme at higher orders will be presented.

1. Introduction

DiscoTEX is a numerical algorithm which computes numerical weak-form solutions to distributionally sourced partial differential equations via the method of lines framework. Spatial discretisation is performed by correcting Lagrange integration formula via discontinuous collocation methods and time-integration is computed via implicit-turned-explicit Hermite formulae corrected to the discontinuous case.

In the first paper [1], we have shown how this algorithm could be used for the modelling of E(X)tremely and (E)xtreme Mass-Ratio-Inspirals (X)/(E)MRIs in comparison to previous time-domain numerical methods used. Highly accurate numerical solutions were obtained provided three numerical control factors are optimised via comprehensive numerical convergence tests. These user-specifiable optimisation factors are:

1. [CTRL F1] - Number of N nodes;
2. [CTRL F2] - Number of J jumps;
3. [CTRL F3] - $\Delta\tau$, timestep size.

Our results were further complemented by demonstrating DiscoTEX's superior performance against its closest relatives: the parent DiscoIMP - using the purely implicit Hermite scheme for numerical integration, and DiscoREX - which uses the purely explicit Runge-Kutta scheme. Finally, we computed numerical solutions to the governing equations for a point particle on a circular geodesic in a Schwarzschild black hole with higher-order time-integration IMTEX Hermite schemes via DiscoTEX, see ref. [1] Table 8. From our results is clear, that with the current software implementation, increasing the algorithm's order did not change the accuracy within the same numerical setup, while taking significantly longer as we increased the order of

numerical integration.

In this work, we provide the full details of the DiscoTEX (and relatives) algorithm for higher orders of numerical convergence via the computation and comparison of the numerical solutions to the distributionally-source wave equation which possesses exact solutions [2, 3, 4, 5]. All the machinery necessary for the inclusion of higher-order time jumps emerging from a point particle prescribing a time-dependent trajectory is detailed. It is further observed the convergence rates are as expected for higher-order time-integration schemes and thus, the work may find application in problems with long evolutions that don't require a second interpolation step (computed by the DiscoTEX "interpolator") such as XMRI waveform modelling and black hole spectroscopy [6].

The paper is organised as follows. In Section 2 we will describe the discontinuous time-integration method at order-12 and compare it to other algorithms as used in [1, 7, 8]. In Section 3 we will compute the numerical weak-form solutions to distributionally sourced wave equations with DiscoTEX at higher orders and compare all algorithms. Finally, we conclude in Section 4 discussing potential applications for higher order DiscoTEX's schemes.

2. The DiscoTEX numerical recipe in a nutshell

In this work we will demonstrate how to compute numerical weak-form solutions [1, 2, 3, 4, 5] to distributionally sourced PDEs of Type I described in the hyperboloidal coordinate chart $(t, x) \rightarrow (t(\tau, \sigma), x(\sigma))$ as,

$$\text{Type I: } \square\Psi[\tau, \sigma] = F(\tau)\delta'(\sigma - \xi_p) + G(\tau)\delta(\sigma - \xi_p), \quad (1)$$

where $\theta = \gamma^2(t - x\xi_p - |x - x_p|)$, $G(\tau) = \cos(\tau) = -iF(\tau)$ and sgn refers to the signum function with the (t, x) coordinates

Email address: lidiajgomesdasilva.io, lidiajoana@pm.me ()

mapped into the new chart. As showed by [3] (albeit in the (t, x) coordinate chart) this admits the following exact solution:

$$\text{Type I: } \square\Psi(t, x) = G(t)\delta(x - r_p) + F(t)\delta'(x - r_p), \quad (2)$$

$$\Psi(t, x) = -\frac{1}{2} \sin \theta + \frac{1}{2} i \gamma^2 [\dot{r}_p + \text{sgn}(x - r_p)] \cos \theta. \quad (3)$$

These equations admit numerical weak-form solutions via the ansatz:

$$\Psi(\tau, \sigma) = \Psi^+(\tau, \sigma)\Theta[\sigma - \xi_p(\tau)] + \Psi^-(\tau, \sigma)\Theta[\xi_p(\tau) - \sigma], \quad (4)$$

where $\Theta(z)$ is the Heaviside function defined as

$$\Theta(z) = \begin{cases} 1 & \text{for } z > 0, \\ \frac{1}{2} & \text{for } z = 0, \\ 0 & \text{for } z < 0. \end{cases} \quad (5)$$

A time-dependent jump is,

$$[[\Psi]](\tau) = \Psi^+(\tau, \xi_p(\tau)) - \Psi^-(\tau, \xi_p(\tau)). \quad (6)$$

2.1. Method-of-lines framework

The first step to solve equation 4, numerically, is to start by reducing the problem to a coupled system of first-order ordinary differential equations in time. The numerical problem reduces to a 1+1D problem illustrated by

$$\partial_\tau \mathbf{U} = \mathbf{L} \cdot \mathbf{U} + \mathcal{S}, \quad \mathbf{U} = \begin{pmatrix} \Psi \\ \Pi \end{pmatrix}, \quad (7)$$

where \mathbf{L} is a spatial differential operator and $\Psi(\tau, \sigma)$, $\Pi(\tau, \sigma)$ are the field variables and their partial derivatives with respect to time. DiscoTEX tackles this system by correcting Lagrange and Hermite interpolation formulae by building discontinuous discretisations in both the spatial and temporal directions. In the following sections, we briefly detail this and refer the reader to [1] where they have been comprehensively explained.

2.2. Spatial discretisation via discontinuous collocation methods

$\mathbf{U}(\tau, \sigma)$, can be discretised in space such that, effectively the numerical system to be solved is effectively time-dependent, as $\mathbf{U}(\tau, \sigma) \rightarrow \mathbf{U}(\tau, \sigma_i) := \mathbf{U}_i(\tau) = \mathbf{U}(\tau)$ where $a \leq \sigma_i \leq b$ with the collocation nodes ranging from $0 < i < N$.

Essentially, we admit the weak-form solution given in equation (4) and work with the generic interpolating piecewise polynomial

$$p(\sigma) = \sum_{j=0}^N \left[\Psi_j + \Delta\Psi(\sigma_j - \xi_p; \sigma - \xi_p) \right] \pi_j(\sigma), \quad (8)$$

where $\pi(\sigma)$ is the Lagrange basis polynomial (LBP) given as

$$\pi_j(\sigma) = \prod_{\substack{k=0, \\ k \neq j}}^N \frac{\sigma - \sigma_k}{\sigma_j - \sigma_k}, \quad (9)$$

and the $\Delta\Psi$ function is given by

$$\begin{aligned} \Delta\Psi(\sigma_j - \xi_p; \sigma - \sigma_p) &= \\ &= \left[\Theta(\sigma_i - \xi_p) - \Theta(\sigma_j - \xi_p) \right] g(\sigma_j - \xi_p) \text{ when } \sigma = \sigma_i. \end{aligned} \quad (10)$$

The LBP is built using suitable collocation nodes as it was explained in [1, 7]. In the work that follows we will use Chebyshev pseudospectral collocation nodes as defined in Section 3 of [1]. The function $g(\sigma_j - \xi_p)$ is defined as

$$g(\sigma_j - \xi_p) = \sum_{m=0}^M \frac{J_m}{m!} (\sigma_j - \xi_p)^m. \quad (11)$$

Our master field variables Ψ and Π , as defined in equation (7), is then effectively approximated as

$$\Psi(\tau, \sigma) \approx \sum_{j=0}^N \left[\Psi_j(\tau) + \Delta\Psi(\sigma_j - \xi_p(\tau); \sigma - \xi_p(\tau)) \right] \pi_j(\sigma). \quad (12)$$

To be precise, all the differential operators in equation (1) and further specified in equations ((54)-(58)), are discretised as,

$$\partial_\sigma^n(\tau, \sigma) \Psi|_{\sigma=\sigma_i} = p^{(n)}(\sigma) = \sum_{j=0}^N D_{ij}^{(n)} \Psi_j + s_i^{(n)}(\tau), \quad (13)$$

where $s_i^{(n)}(\tau)$ is given as

$$s_i^{(n)}(\tau) = \sum_{j=0}^N D_{ij}^{(n)} \Delta\Psi(\sigma_j - \xi_p(\tau); x_i - \xi_p(\tau)) \quad (14)$$

and the user-specifiable high-order jumps in equation (11) obtained through the computation of the higher-order recurrence relation given as

$$\begin{aligned} J_{m+2}(\tau) &= -\bar{\gamma}^2 \left[\sum_{k=0}^m \binom{m}{k} \left(\varepsilon^{(k)}(\xi_p) J_{m+1-k} + \iota^{(k)}(\xi_p) J_{m+1-k} \right. \right. \\ &\quad \left. \left. - V^{(k)}(\xi_p) J_{m-k} + \rho^{(k)}(\xi_p) (J_{m-k} - \dot{\xi}_p J_{m+1-k}) \right. \right. \\ &\quad \left. \left. + \Gamma^{(k)} (J_{m-k} - 2\dot{\xi}_p J_{m+1-k} - \ddot{\xi}_p J_{m+1-k}) \right) \right. \\ &\quad \left. + \sum_{k=1}^m \binom{m}{k} \left(\dot{\xi}_p^2 \Gamma^{(k)}(\xi_p) + \dot{\xi}_p \varepsilon^{(k)}(\xi_p) + \chi^{(k)}(\xi_p) \right) J_{m+2-k} \right]. \end{aligned} \quad (15)$$

where here for simplicity the time dependence on the RHS of the jumps has been suppressed and we have, $\bar{\gamma}^{-2} = (\dot{\xi}_p^2 \Gamma(\xi_p) - \dot{\xi}_p \varepsilon(\xi_p) - \chi(\xi_p))$. This machinery introduces two user-specifiable numerical optimisation control-factors that will need to be subjected to a comprehensive numerical convergence study [1, 7, 8],

1. [CTRL F1] - Number of nodes, N;
2. [CTRL F2] - Number of jumps, J.

2.3. Discontinuous time-integration via Hermite interpolation at higher-orders

We now extend the procedure described in [1] to order-12 and start by considering the first-order differential equation,

$$\frac{dy}{dt} = f(t, y(t)), \quad (16)$$

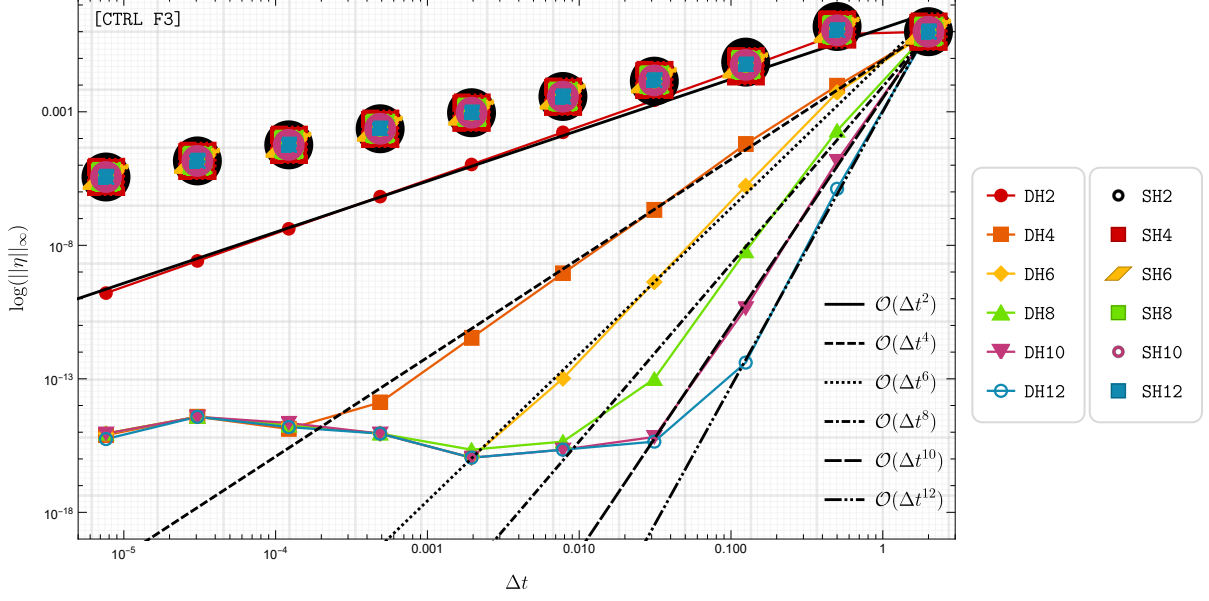


Figure 1: Numerical error associated with the numerical evaluation of the integral in equation (48) with the numerical scheme of equations ((A.1) - (A.10)) corrected by incorporating the discontinuous behaviour through the discontinuous time-integration rules given through equations ((A.7) - (47)). For numerical integration schemes of 2nd to 12th order numerical convergence in the same order is observed as given by the lines DH2-DH12. Inaccurate results are recorded for a smooth integrator as given by line SH2-SH12. The computational wall-clock times for the simulations are given in Table 1.

on a small time interval $[t_v, t_{v+1}]$. Applying the fundamental theorem of calculus we have,

$$y(t_{v+1}) - y(t_v) = \int_{t_v}^{t_{v+1}} f(t, y(t)) dt. \quad (17)$$

As demonstrated in [1] the discontinuous behaviour is incorporated by constructing the interpolant as a piecewise polynomial,

$$f(t, y(t)) \approx p(t) = p_+(t)\Theta(t - t_x) + p_-(t)\Theta(t_x - t), \quad (18)$$

where t_x is the point where the function is discontinuous such that $t_x \in [t_v, t_{v+1}]$ and f is approximated as p_+ in $[t_x, t_{v+1}]$ and p_- in $[t_v, t_x]$. Explicitly we have,

$$p_+(t) = a_0 + a_1 t + a_2 t^2 + a_3 t^3 + a_4 t^4 + a_5 t^5 + a_6 t^6 + a_7 t^7 + a_8 t^8 + a_9 t^9 + a_{10} t^{10} + a_{11} t^{11}, \quad (19)$$

$$p_-(t) = b_0 + b_1 t + b_2 t^2 + b_3 t^3 + b_4 t^4 + b_5 t^5 + b_6 t^6 + b_7 t^7 + b_8 t^8 + b_9 t^9 + b_{10} t^{10} + b_{11} t^{11}. \quad (20)$$

$$(21)$$

Even though we have 24 unknown coefficients, the jump conditions are known and thus the following collocation conditions are imposed:

$$p_-(t_v) = f_v, p_+(t_{v+1}) = f_{v+1}, \quad (22)$$

$$p'_-(t_v) = df_v, p'_+(t_{v+1}) = df_{v+1}, \quad (23)$$

$$p''_-(t_v) = ddf_v, p''_+(t_{v+1}) = ddf_{v+1}, \quad (24)$$

$$p'''_-(t_v) = dddf_v, p'''_+(t_{v+1}) = dddf_{v+1}, \quad (25)$$

$$p_-^{(4)}(t_v) = d4f_v, p_+^{(4)}(t_{v+1}) = d4f_{v+1}, \quad (26)$$

$$p_-^{(5)}(t_v) = d5f_v, p_+^{(5)}(t_{v+1}) = d5f_{v+1}, \quad (27)$$

$$p_-^{(6)}(t_v) = d6f_v, p_+^{(6)}(t_{v+1}) = d6f_{v+1}, \quad (28)$$

$$p_-^{(7)}(t_v) = d7f_v, p_+^{(7)}(t_{v+1}) = d7f_{v+1}, \quad (29)$$

$$p_-^{(8)}(t_v) = d8f_v, p_+^{(8)}(t_{v+1}) = d8f_{v+1}, \quad (30)$$

$$p_-^{(9)}(t_v) = d9f_v, p_+^{(9)}(t_{v+1}) = d9f_{v+1}, \quad (31)$$

$$p_-^{(10)}(t_v) = d10f_v, p_+^{(10)}(t_{v+1}) = d10f_{v+1}, \quad (32)$$

$$p_-^{(11)}(t_v) = d11f_v, p_+^{(11)}(t_{v+1}) = d11f_{v+1}, \quad (33)$$

$$p_+(t_x) - p_-(t_x) = \mathbf{J}_0, \quad (34)$$

$$p'_+(t_x) - p'_-(t_x) = \mathbf{J}_1, \quad (35)$$

$$p''_+(t_x) - p''_-(t_x) = \mathbf{J}_2, \quad (36)$$

$$p'''_+(t_x) - p'''_-(t_x) = \mathbf{J}_3, \quad (37)$$

$$p_+^{(4)}(t_x) - p_-^{(4)}(t_x) = \mathbf{J}_4, \quad (38)$$

$$p_+^{(5)}(t_x) - p_-^{(5)}(t_x) = \mathbf{J}_5, \quad (39)$$

$$p_+^{(6)}(t_x) - p_-^{(6)}(t_x) = \mathbf{J}_6, \quad (40)$$

$$p_+^{(7)}(t_x) - p_-^{(7)}(t_x) = \mathbf{J}_7, \quad (41)$$

$$p_+^{(8)}(t_x) - p_-^{(8)}(t_x) = \mathbf{J}_8, \quad (42)$$

$$p_+^{(9)}(t_x) - p_-^{(9)}(t_x) = \mathbf{J}_9, \quad (43)$$

$$p_+^{(10)}(t_x) - p_-^{(10)}(t_x) = \mathbf{J}_{10}, \quad (44)$$

$$p_+^{(11)}(t_x) - p_-^{(11)}(t_x) = \mathbf{J}_{11}. \quad (45)$$

With these 24 conditions, we can now solve for the 24 polynomial coefficients highlighted in equations ((19), (21)) as a linear system of algebraic equations. Integrating both of the piecewise polynomials yields

$$\begin{aligned}
f(t)_{\text{DH12}} &= \frac{\Delta t}{2} \left(f(t_n) + f(t_{n+1}) \right) + \frac{5\Delta t^2}{44} \left(\dot{f}(t_n) - \dot{f}(t_{n+1}) \right) \\
&+ \frac{\Delta t^3}{66} \left(\ddot{f}(t_n) + \ddot{f}(t_{n+1}) \right) + \frac{\Delta t^4}{792} \left(\frac{d^3 f(t_n)}{dt^3} - \frac{d^3 f(t_{n+1})}{dt^3} \right) \\
&+ \frac{\Delta t^5}{15840} \left(\frac{d^4 f(t_n)}{dt^4} + \frac{d^4 f(t_{n+1})}{dt^4} \right) + \frac{\Delta t^6}{665280} \left(\frac{d^5 f(t_n)}{dt^5} - \frac{d^5 f(t_{n+1})}{dt^5} \right) \\
&+ \mathbf{J}_{\text{H12}}(\Delta t_x, \Delta t), \tag{46}
\end{aligned}$$

where $\mathbf{J}_{\text{H12}}(\Delta t_x, \Delta t)$ is given by,

$$\begin{aligned}
\mathbf{J}_{\text{H12}}(\Delta t_x, \Delta t) &= \frac{1}{2}(\Delta t - 2\Delta t_x)\mathbf{J}_0 + \frac{1}{44}(5\Delta t^2 - 22\Delta t\Delta t_x + 22\Delta t_x^2) \\
&+ \frac{1}{132}(\Delta t - 2\Delta t_x)(2\Delta t^2 - 11\Delta t\Delta t_x + 11\Delta t_x^2)\mathbf{J}_2 \\
&+ \frac{1}{792}(\Delta t^4 - 12\Delta t^3\Delta t_x + 45\Delta t^2\Delta t_x^2 - 66\Delta t\Delta t_x^3 + 33\Delta t_x^4)\mathbf{J}_3 \\
&+ \frac{1}{15840}(\Delta t - 2\Delta t_x)(\Delta t^4 - 18\Delta t^3\Delta t_x \\
&+ 84\Delta t^2\Delta t_x^2 - 132\Delta t\Delta t_x^3 + 66\Delta t_x^4)\mathbf{J}_4 \\
&+ \frac{1}{665280}(\Delta t^6 - 42\Delta t^5\Delta t_x + 420\Delta t^4\Delta t_x^2 - 1680\Delta t^3\Delta t_x^3 \\
&+ 3150\Delta t^2\Delta t_x^4 - 2772\Delta t\Delta t_x^5 + 924\Delta t_x^6)\mathbf{J}_5 \\
&+ \frac{1}{30240}(\Delta t - \Delta t_x)\Delta t_x(\Delta t^4 - 14\Delta t^3\Delta t_x + 56\Delta t^2\Delta t_x^2 \\
&- 84\Delta t\Delta t_x^3 + 42\Delta t_x^4)\mathbf{J}_5 \\
&- \frac{1}{665280}(\Delta t - 2\Delta t_x)(\Delta t - \Delta t_x)\Delta t_x \\
&\times (\Delta t^4 - 18\Delta t^3\Delta t_x + 45\Delta t^2\Delta t_x^2 - 132\Delta t\Delta t_x^3 + 66\Delta t_x^4)\mathbf{J}_6 \\
&+ \frac{1}{1330560}(\Delta t - \Delta t_x)^2\Delta t_x^2(\Delta t^4 - 12\Delta t^3\Delta t_x + 45\Delta t^2\Delta t_x^2 \\
&- 66\Delta t\Delta t_x^3 + 33\Delta t_x^4)\mathbf{J}_7 \\
&+ \frac{1}{7983360}(\Delta t - 2\Delta t_x)(\Delta t - \Delta t_x)^3\Delta t_x^3(2\Delta t^2 - 11\Delta t\Delta t_x + 11\Delta t_x^2)\mathbf{J}_8 \\
&+ \frac{1}{79833600}(\Delta t - \Delta t_x)^4\Delta t_x^4(5\Delta t^2 - 22\Delta t\Delta t_x + 22\Delta t_x^2)\mathbf{J}_9 \\
&- \frac{1}{79833600}(\Delta t - 2\Delta t_x)(\Delta t - \Delta t_x)^5\Delta t_x^5\mathbf{J}_{10} \\
&+ \frac{1}{479001600}(\Delta t - \Delta t_x)^6\Delta t_x^6\mathbf{J}_{11}, \tag{47}
\end{aligned}$$

With the aid of Appendix A.1 we study the numerical rate of convergence of the discontinuous Hermite interpolation scheme by computing numerical solutions from 2nd to 12th order to the following time-dependent Legendre polynomial,

$$f(t) = P_5(t)\Theta(t) + Q_5(t)\Theta(t), \tag{48}$$

where $P_5(t)$, $Q_5(t)$ are the fifth Legendre polynomials of the first and second kind respectively. Introducing a discontinuity at $t_x = 0$ in the interval $t \in [-0.55, 0.45]$, equation (48) admits

Order of NDH	Wall-clock times, s
Order 2, NDH2	4.15227
Order 4, NDH4	55.5743
Order 6, NDH6	122.499
Order 8, NDH8	199.787
Order 10, NDH10	268.464
Order 12, NDH12	348.885

Table 1: Total wall-clock computational running time to perform the numerical convergence test summarised on Figure 1.

the following analytical jumps,

$$\mathbf{J}_0 = \frac{8}{15}, \mathbf{J}_1 = \frac{15}{8}, \mathbf{J}_2 = -16, \mathbf{J}_3 = -\frac{105}{2}, \tag{49}$$

$$\mathbf{J}_4 = 384, \mathbf{J}_5 = 945, \mathbf{J}_6 = -3840, \mathbf{J}_7 = 0, \tag{50}$$

$$\mathbf{J}_8 = -46080, \mathbf{J}_9 = 0, \mathbf{J}_{10} = -1935360, \mathbf{J}_{11} = 0. \tag{51}$$

Integrating analytically the above polynomial in the interval $t \in [-0.55, 0.45]$ we get $\approx 0.1125883303464025$. From Figure 1 it is observed that the error associated with the discontinuous time-integration rules scales with the respective order of the scheme that is used. To further complement our results we also include a comparison if only a smooth time-integration was used, as described by equations ((A.1) - (A.10)), now corrected in the scheme by incorporating the discontinuous behaviour through the discontinuous time-integration rules given through equations ((A.7) - (47)). To further investigate the effect increasing the order of the integrator had on numerical results we computed the total simulation running time to compute the numerical data showcased in Figure 1 for all the 12th order discontinuous Hermite interpolation schemes that were used. As it is observed in Table 1 there is a significant increase in the total simulation running time.

A third user-specifiable numerical optimisation control-factor emerges [1, 7, 8]

1. [CTRL F1] - Number of N nodes;
2. [CTRL F2] - Number of J jumps;
3. [CTRL F3] - $\Delta\tau/\Delta t$, time step-size.

As we noted in [1] the jumps in the time direction, \mathbf{J} are fixed and determined by the order of the discontinuous time-integration algorithm as evidenced by equations ((46), (47)) and the respective equations for the different order integrators given in Appendix A.1.

3. Numerical weak-form solutions to distributionally sourced partial differential equations via DiscoTEX - generalisation to higher orders

3.1. DiscoTEX at higher-orders: Algorithm description

It will now be demonstrated how DiscoTEX is applied to solve the distributionally-sourced wave-equation of Type I [1] given as

$$\square\Psi(\tau, \sigma) = \mathcal{S}(\tau, \sigma), \tag{52}$$

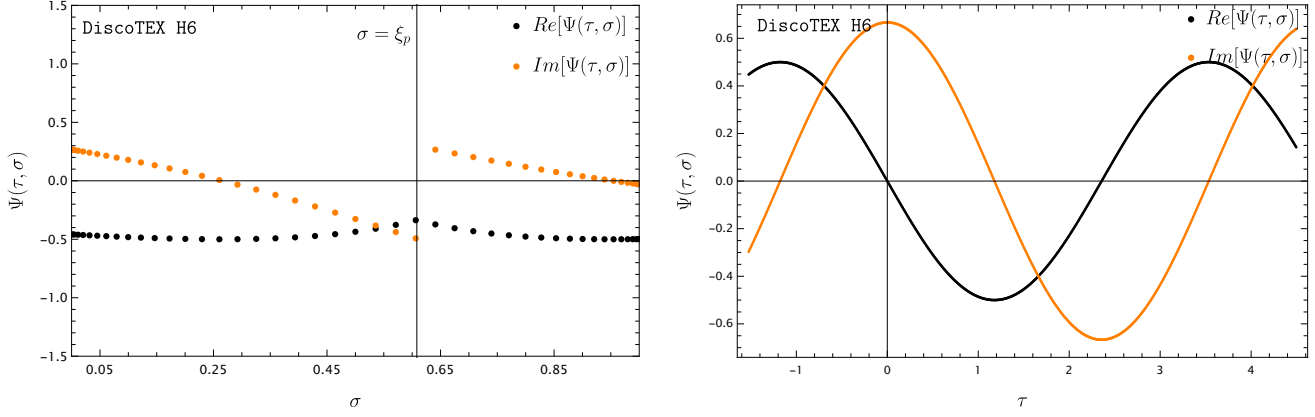


Figure 2: Numerical weak-form solution to $\Psi(\tau, \sigma)$ obtained via the `DiscoTEX H6` 6th-order algorithm. **Left:** Numerical field $\Psi(\tau, \sigma)$ for a point-particle in time-dependent linear motion $\xi_p(\tau_c)$, where v is the particle's velocity. Specifically, here $\xi_p \approx 0.608$ at the coordinate-time $\tau_c \approx 0.876$ and $v = 1/4$. **Right:** Waveform for the point-particle computed on the numerical domain $\sigma \in [0, 1]$ and $\tau \in [-1.52, 4.50]$. As expected the result matches that observed for the solution obtained with `DiscoTEX H4` 4th-order numerical algorithm [1].

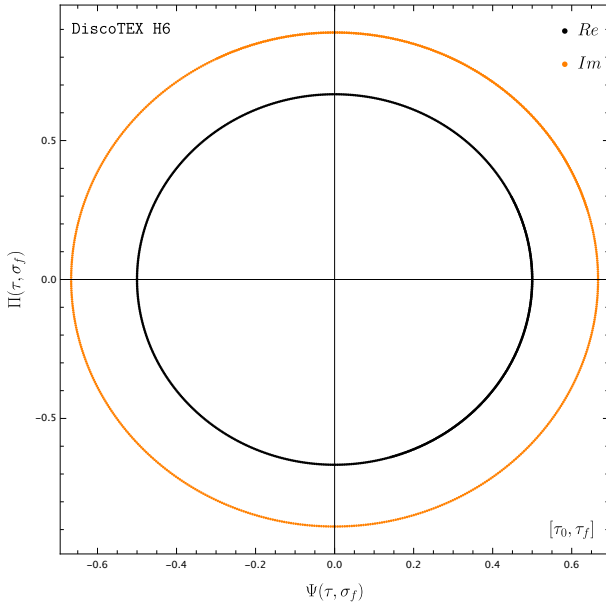


Figure 3: Phase portrait for the numerical weak-form solution obtained via `DiscoTEX H6` with a 6th-order `IMTEX Hermite H6` time integrator in the (τ, σ) hyperboloidal chart. The numerical weak-form solutions to the field $\Psi(\tau, \sigma_f)$, $\Pi(\tau, \sigma_f)$ are evaluated in the numerical time interval $\tau \in [-1.52, 4.50]$ at the last grid point. As reminded in [1] here we too point out that unlike in [7], Figure 2, uses the exact solutions as initial data, whereas in our previous work, we used trivial initial data, thus not requiring the monitoring of an extra user-specifiable control factor.

with,

$$\square\Psi = \left(-\Gamma(\sigma)\partial_\tau^2 + \varepsilon(\sigma)\partial_\sigma\partial_\tau + \varrho(\sigma)\partial_\tau + \chi(\sigma)\partial_\sigma^2 + \iota(\sigma)\partial_\sigma \right)\Psi. \quad (53)$$

The coefficients are specified by

$$\Gamma(\sigma) = -4\sigma^2(-1 + \sigma^2), \quad (54)$$

$$\varepsilon(\sigma) = -4(-1 + \sigma)\sigma^2(-1 + 2\sigma^2), \quad (55)$$

$$\varrho(\sigma) = -8(-1 + \sigma)\sigma^3, \quad (56)$$

$$\chi(\sigma) = -4(-1 + \sigma)^2\sigma^4, \quad (57)$$

$$\iota(\sigma) = -4(-1 + \sigma)\sigma^3(-2 + 3\sigma), \quad (58)$$

where, as in [1, 7], it's emphasised that the function $\chi(\sigma)$ vanishes at the boundaries where $\sigma = \{0, 1\}$, reflecting the outflow behaviour automatically enforced by this hyperboloidal slicing at the future null infinity and the horizon, respectively. The term $\mathcal{S}(\tau)$ is place-hold notation to denote the distributionally source function as only a time-dependent function as before. We will shortly explain how this is handled. As explained in Section 2.1 we work via the method-of-lines framework,

$$\frac{d\mathbf{U}}{d\tau} = \mathbf{L} \cdot \mathbf{U} + \mathcal{S} + \Upsilon, \quad \mathbf{U} = \begin{pmatrix} \Psi(\tau) \\ \Pi(\tau) \end{pmatrix}, \quad \mathcal{S} = \begin{pmatrix} 0 \\ \mathbf{s}_\Psi(\tau) + \mathbf{s}_\Pi(\tau) \end{pmatrix}, \quad \Upsilon = \begin{pmatrix} \Upsilon_\Psi(\tau) \\ \Upsilon_\Pi(\tau) \end{pmatrix}, \quad (59)$$

with the evolution operator \mathbf{L} described as,

$$\mathbf{L}_1 = \frac{1}{\Gamma(\sigma)} \left(\chi(\sigma)\partial_\sigma^2 + \iota(\sigma)\partial_\sigma \right), \quad (60)$$

$$\mathbf{L}_2 = \frac{1}{\Gamma(\sigma)} \left(\varepsilon(\sigma)\partial_\sigma - \varrho(\sigma) \right), \quad (61)$$

where, for convenience as described in [1, 7], the tilde notation is introduced to denote division of the coefficients in the operators by $\Gamma(\sigma)$, e.g., $\tilde{\varepsilon}(\sigma) = \varepsilon(\sigma)/\Gamma(\sigma)$. As motivated in

[1] we choose to work with the hyperboloidal chart (τ, σ) via the coordinate map $(t \rightarrow t(\tau, \sigma), x \rightarrow x(\sigma))$ described by the “scri-fixing” technique [9, 10],

$$t = \tau - H(\sigma), \quad x = \frac{1}{2} \left(\frac{1}{\sigma} + \ln(1 - \sigma) - \ln \sigma \right), \quad (62)$$

where height function $H(\sigma)$ is given by,

$$H(\sigma) = \frac{1}{2} \left[\ln(1 - \sigma) - \frac{1}{\sigma} + \ln \sigma \right] \quad (63)$$

as originally introduced by [11, 12, 13, 14].

The term Υ is defined as,

$$\begin{pmatrix} \Upsilon_\Psi(\tau) = [[\Psi]]_i \Xi_i = J_0(\tau) * \Xi_i \\ \Upsilon_\Pi(\tau) = [[\Pi]]_i \Xi_i = \mathbb{J}_0(\tau) * \Xi_i \end{pmatrix}. \quad (64)$$

The reader is directed to Appendix A.2, where the explicit form of the initialising jumps, $J_0(\tau), J_1(\tau)$ are given. The time jumps are obtained as

$$\mathbb{J}(\tau) = \mathbb{J}_m(\tau) = \partial_\tau(J_m(\tau)) - \dot{\xi}_p(\tau) J_{m+1}(\tau), \quad (65)$$

$$\mathbb{J}(\tau)|_{m=0} = \mathbb{J}_0(\tau) = \partial_\tau(J_0(\tau)) - \dot{\xi}_p(\tau) J_1(\tau). \quad (66)$$

$[[\Psi]]_i$ is as defined in equation (6), and $[[\Pi]]_i$ is given by

$$[[\Pi]]_i = \Pi^+(\tau, \xi_p(\tau)) - \Pi^-(\tau, \xi_p(\tau)), \quad \tau \rightarrow \frac{\sigma_i}{v} \quad (67)$$

$$\Xi_i = \Theta(\tau_{n+1} - \tau_i) \Theta(\tau_i - \tau_n), \quad (68)$$

where Θ is as defined in equation (5) and Ξ_i acts as a switch which turn on these corrections in the time direction for both the $\Psi(\tau)$ and $\Pi(\tau)$ master functions when the particle worldline $x_p(t)$ crosses the i -th grid-point as they are integrated through DiscoTEX at a time $\tau_i \in [\tau_n, \tau_{n+1}] : \xi_p(\tau) = \sigma_i$. We now need to correct the discontinuities in space with the machinery outlined in Section 2.2. Specifically we correct equations ((77), (78)) which contribute to the corrected \mathbf{L}_1 operator associated with the master function $\Psi(\tau, \sigma)$ and equation (79) contributes to the corrected \mathbf{L}_2 operator. The vector \mathcal{S} in (59) concretely is,

$$\tilde{\mathbf{s}}(\tau) = \begin{pmatrix} 0 \\ \tilde{s}_{\Psi,(1)} + \tilde{s}_{\Psi,(2)} + \tilde{s}_{\Pi,(1)} \end{pmatrix}, \quad (69)$$

where the subscripts (1,2) denotes 1st/2nd- derivative with respect to space. However, as demonstrated in [1] higher-order time-derivatives of this source term are necessary, as the orders of the time-integration scheme used are increased. In this work, we use a sixth-order Hermite time-integration rule

given as,

$$\begin{aligned} \mathbf{U}_{n+1} - \mathbf{U}_n &= \int_{\tau_n}^{\tau_{n+1}} (\mathbf{L} \cdot \mathbf{U} + \mathcal{S}) d\tau \\ &= \frac{\Delta\tau}{2} \mathbf{L} \cdot (\mathbf{U}_n + \mathbf{U}_{n+1}) + \frac{\Delta\tau}{2} (\mathcal{S}_n + \mathcal{S}_{n+1}) \\ &\quad + \frac{\Delta\tau^2}{10} \mathbf{L} \cdot (\dot{\mathbf{U}}_n - \dot{\mathbf{U}}_{n+1}) + \frac{\Delta\tau^2}{10} (\dot{\mathcal{S}}_n - \dot{\mathcal{S}}_{n+1}) \\ &\quad + \frac{\Delta\tau^3}{120} \mathbf{L} \cdot (\ddot{\mathbf{U}}_n + \ddot{\mathbf{U}}_{n+1}) + \frac{\Delta\tau^3}{120} (\ddot{\mathcal{S}}_n + \ddot{\mathcal{S}}_{n+1}) \\ &= \frac{\Delta\tau}{2} (\mathbf{U}_n + \mathbf{U}_{n+1}) + \frac{\Delta\tau}{2} (\mathcal{S}_n + \mathcal{S}_{n+1}) \\ &\quad + \frac{\Delta\tau^2}{10} \mathbf{L} \cdot (\mathbf{L} \cdot \mathbf{U}_n - \mathbf{L} \cdot \mathbf{U}_{n+1}) + \frac{\Delta\tau^2}{10} \mathbf{L} \cdot (\mathcal{S}_n - \mathcal{S}_{n+1}) \\ &\quad + \frac{\Delta\tau^3}{120} \mathbf{L} \cdot (\mathbf{L} \cdot \mathbf{L} \cdot \mathbf{U}_n + \mathbf{L} \cdot \mathbf{L} \cdot \mathbf{U}_{n+1}) \\ &\quad + \frac{\Delta\tau^3}{120} \mathbf{L} \cdot (\mathbf{L} \cdot \mathcal{S}_n + \mathbf{L} \cdot \mathcal{S}_{n+1}) + \frac{\Delta\tau^3}{120} \mathbf{L} \cdot (\dot{\mathcal{S}}_n + \dot{\mathcal{S}}_{n+1}) \\ &\quad + \frac{\Delta\tau^2}{10} (\dot{\mathcal{S}}_n - \dot{\mathcal{S}}_{n+1}) + \frac{\Delta\tau^3}{120} (\ddot{\mathcal{S}}_n + \ddot{\mathcal{S}}_{n+1}), \end{aligned} \quad (70)$$

where the following replacement was used,

$$\begin{aligned} \mathbf{U}^{(2)} &= \frac{d}{d\tau} [\mathbf{L} \cdot \mathbf{U} + \mathcal{S}], \\ &= \mathbf{L} \cdot (\mathbf{L} \cdot \mathbf{U} + \mathcal{S}) + \frac{d\mathcal{S}}{d\tau}, \\ &= \mathbf{L} \cdot \mathbf{L} \cdot \mathbf{U} + \mathbf{L} \cdot \mathcal{S} + \mathcal{S}^{(1)}, \end{aligned} \quad (71)$$

and the superscript (2) denotes the 2nd-order derivative with respect to the time coordinate. In Appendix A.3 we give this necessary transformation for schemes of higher-order i.e. 8th- to 12th- order, throughout equations ((A.16)-(A.24)). With a sixth order algorithm the following time-derivative source terms are necessary,

$$\tilde{\mathbf{s}}^{(1)}(\tau) = \begin{pmatrix} 0 \\ \tilde{s}_{\Psi,(1)}^{(1)} + \tilde{s}_{\Psi,(2)}^{(1)} + \tilde{s}_{\Pi,(1)}^{(1)} \end{pmatrix}, \quad (72)$$

and

$$\tilde{\mathbf{s}}^{(2)}(\tau) = \begin{pmatrix} 0 \\ \tilde{s}_{\Psi,(2)}^{(2)} + \tilde{s}_{\Psi,(2)}^{(2)} + \tilde{s}_{\Pi,(1)}^{(2)} \end{pmatrix}. \quad (73)$$

The differential operators corrected with the discontinuous collocation algorithm are given by,

$$\begin{aligned} &\tilde{\chi}(\sigma) \partial_\sigma^2 \Psi \Big|_{\sigma=\sigma_i} \\ &= \sum_{j=0}^N \left(\tilde{\chi}(\sigma_i) \times D_{(2)} \right)_{ij} [\Psi_j + \Delta\Psi(\sigma_j - \sigma_p; \sigma_i - \sigma_p) \\ &\quad + \Delta\Psi^{(1)}(\sigma_j - \sigma_p; \sigma_i - \sigma_p) + \Delta\Psi^{(2)}(\sigma_j - \sigma_p; \sigma_i - \sigma_p)], \end{aligned} \quad (74)$$

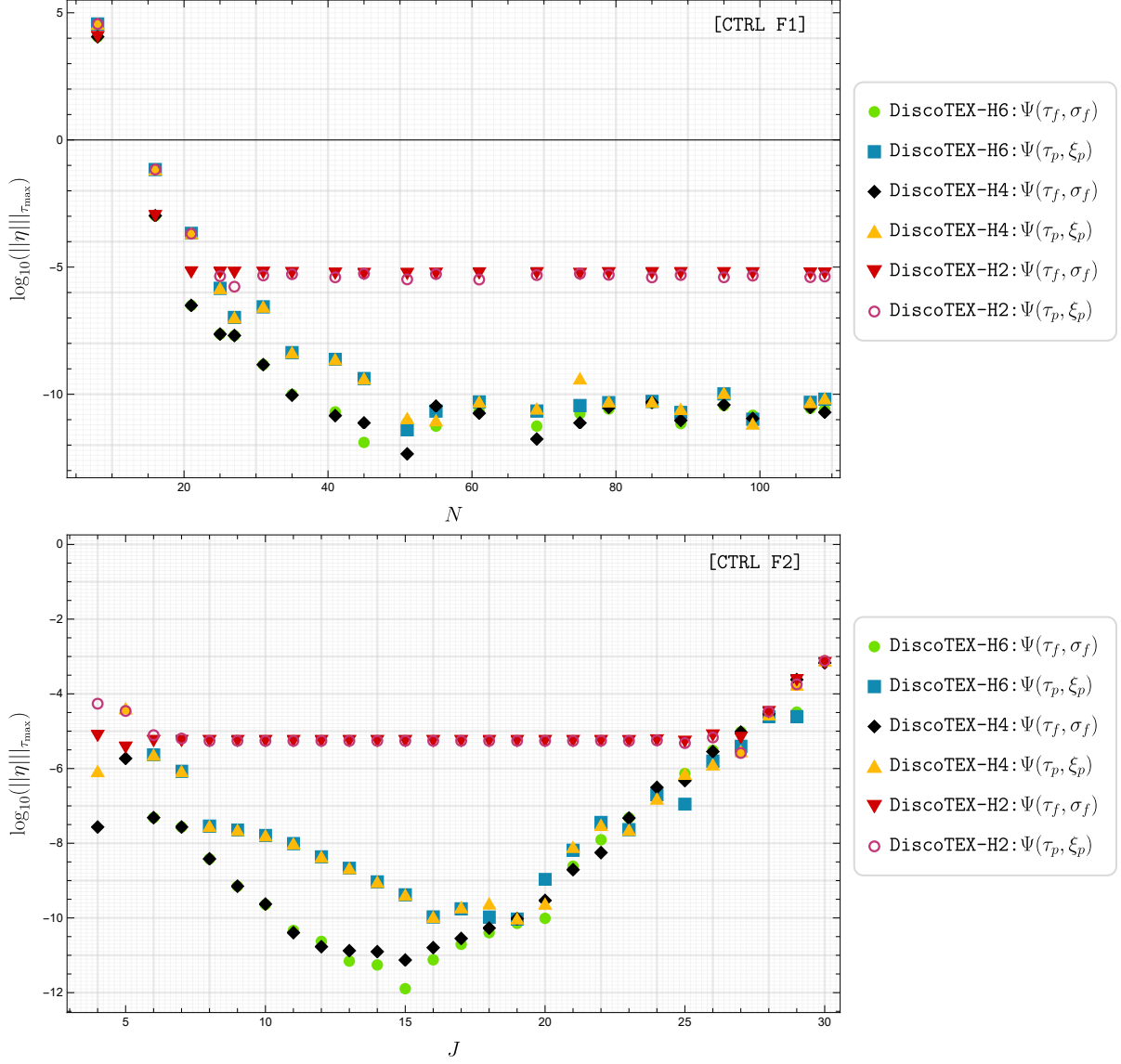


Figure 4: Numerical convergence studies assessing the optimal user-specifiable control factors: number of N nodes - [CTRL F1] (top plot) and number of J jumps - [CTRL F2] (bottom plot). Whereas there is a significant accuracy improvement after the second-order time-integration scheme, the difference between the 4th and 6th time-stepper is marginal for a similar numerical set-up. It is reasonable to pick $N=45$ Chebyshev collocation nodes and $J=19$ jumps.

$$\begin{aligned} \tilde{i}(\sigma)\partial_\sigma\Psi\Big|_{\sigma=\sigma_i} &= \\ &\sum_{j=0}^N \left(\tilde{i}(\sigma_i) \times D_{(1)} \right)_{ij} [\Psi_j + \Delta_\Psi(\sigma_j - \sigma_p; \sigma_i - \sigma_p) \\ &+ \Delta_\Psi^{(1)}(\sigma_j - \sigma_p; \sigma_i - \sigma_p) + \Delta_\Psi^{(2)}(\sigma_j - \sigma_p; \sigma_i - \sigma_p)], \end{aligned} \quad (75)$$

$$\begin{aligned} \tilde{\xi}(\sigma)\partial_\sigma\Pi\Big|_{\sigma=\sigma_i} &= \\ &\sum_{j=0}^N \left(\tilde{\xi}(\sigma_i) \times D_{(1)} \right)_{ij} [\Pi_j + \Delta_\Pi(\sigma_j - \sigma_p; \sigma_i - \sigma_p) \\ &+ \Delta_\Pi^{(1)}(\sigma_j - \sigma_p; \sigma_i - \sigma_p) + \Delta_\Pi^{(2)}(\sigma_j - \sigma_p; \sigma_i - \sigma_p)]. \end{aligned} \quad (76)$$

The explicit form of $\tilde{\mathfrak{s}}(\tau)$ in equation (69) containing all the necessary corrections to the differential operators is

$$\tilde{\mathfrak{s}}_{\Psi,(1)} = \sum_{j=0}^N \left(\tilde{i}(\sigma_i) \times D_{(1)} \right)_{ij} [\Delta_\Psi(\sigma_j - \sigma_p; \sigma_i - \sigma_p)], \quad (77)$$

$$\tilde{\mathfrak{s}}_{\Psi,(2)} = \sum_{j=0}^N \left(\tilde{\chi}(\sigma_i) \times D_{(2)} \right)_{ij} [\Delta_\Psi(\sigma_j - \sigma_p; \sigma_i - \sigma_p)], \quad (78)$$

$$\tilde{\mathfrak{s}}_{\Pi,(1)} = \sum_{j=0}^N \left(\tilde{\xi}(\sigma_i) \times D_{(1)} \right)_{ij} [\Delta_\Pi(\sigma_j - \sigma_p; \sigma_i - \sigma_p)]. \quad (79)$$

Similarly that of $\tilde{\mathfrak{s}}^{(1)}(\tau)$ in equation we have, (72) is

$$\tilde{\mathfrak{s}}_{\Psi,(1)}^{(1)} = \sum_{j=0}^N \left(\tilde{i}(\sigma_i) \times D_{(1)} \right)_{ij} [\Delta_\Psi^{(1)}(\sigma_j - \sigma_p; \sigma_i - \sigma_p)], \quad (80)$$

$$\tilde{\mathfrak{s}}_{\Psi,(2)}^{(1)} = \sum_{j=0}^N \left(\tilde{\chi}(\sigma_i) \times D_{(2)} \right)_{ij} [\Delta_\Psi^{(1)}(\sigma_j - \sigma_p; \sigma_i - \sigma_p)], \quad (81)$$

$$\tilde{\mathfrak{s}}_{\Pi,(1)}^{(1)} = \sum_{j=0}^N \left(\tilde{\xi}(\sigma_i) \times D_{(1)} \right)_{ij} [\Delta_\Pi^{(1)}(\sigma_j - \sigma_p; \sigma_i - \sigma_p)], \quad (82)$$

and finally for $\tilde{\mathfrak{s}}^{(2)}(\tau)$ in equation (73)

$$\tilde{\mathfrak{s}}_{\Psi,(1)}^{(2)} = \sum_{j=0}^N \left(\tilde{i}(\sigma_i) \times D_{(1)} \right)_{ij} [\Delta_\Psi^{(2)}(\sigma_j - \sigma_p; \sigma_i - \sigma_p)], \quad (83)$$

$$\tilde{\mathfrak{s}}_{\Psi,(2)}^{(2)} = \sum_{j=0}^N \left(\tilde{\chi}(\sigma_i) \times D_{(2)} \right)_{ij} [\Delta_\Psi^{(2)}(\sigma_j - \sigma_p; \sigma_i - \sigma_p)], \quad (84)$$

$$\tilde{\mathfrak{s}}_{\Pi,(1)}^{(2)} = \sum_{j=0}^N \left(\tilde{\xi}(\sigma_i) \times D_{(1)} \right)_{ij} [\Delta_\Pi^{(2)}(\sigma_j - \sigma_p; \sigma_i - \sigma_p)]. \quad (85)$$

We further remind the reader as per Section 2.2 the $\Delta_{\Psi,\Pi}$ correction are given as,

$$\begin{aligned} \Delta_\Psi(\sigma_j - \xi_p; \sigma - \sigma_p) &= \\ &= \left[\Theta(\sigma_i - \xi_p) - \Theta(\sigma_j - \xi_p) \right] g_\Psi(\sigma_j - \xi_p) \text{ when } \sigma = \sigma_i, \end{aligned} \quad (86)$$

with $g_\Psi(\sigma_j - \xi_p)$ defined as

$$g_\Psi(\sigma_j - \xi_p) = \sum_{m=0}^M \frac{J_m}{m!} (\sigma_j - \xi_p)^m. \quad (87)$$

Similarly the evolution operator pertaining to the master field $\Pi(\tau, \sigma)$ is corrected to the discontinuous case via,

$$\begin{aligned} \Delta_\Pi(\sigma_j - \xi_p; \sigma - \sigma_p) &= \\ &= \left[\Theta(\sigma_i - \xi_p) - \Theta(\sigma_j - \xi_p) \right] g_\Pi(\sigma_j - \xi_p) \text{ when } \sigma = \sigma_i, \end{aligned} \quad (88)$$

where,

$$g_\Pi(\sigma_j - \xi_p) = \sum_{m=0}^M \frac{\mathbb{J}_m}{m!} (\sigma_j - \xi_p)^m, \quad (89)$$

where the \mathbb{J}_m are computed as explained in (65). Further as per equations ((80)-(85)) we need the following high-order corrections,

$$\begin{aligned} \Delta_\Psi(\sigma_j - \xi_p; \sigma - \sigma_p) &= \\ &= \left[\Theta(\sigma_i - \xi_p) - \Theta(\sigma_j - \xi_p) \right] g_\Psi^{(1)}(\sigma_j - \xi_p) \text{ when } \sigma = \sigma_i, \end{aligned} \quad (90)$$

where

$$\begin{aligned} g_\Psi^{(1)}(\sigma - \xi_p(\tau)) &= \frac{\partial g_\Psi(\sigma - \xi_p(\tau))}{\partial \tau} = \\ &= \frac{\partial}{\partial \tau} \left[\sum_{m=0}^M \frac{J(\tau)}{m!} (\sigma_j - \xi_p(\tau))^m \right] \\ &= \sum_{m=0}^M \left[\frac{1}{m!} \dot{J}(\sigma_j - \xi_p)^m - \frac{m}{m!} \xi_p^{(1)} J(\sigma_j - \xi_p)^{m-1} \right]. \end{aligned} \quad (91)$$

All that is left to do is to correct $\Delta_\Psi^{(2)}$ where the second-order in time g vector is,

$$\begin{aligned} g^{(2)}(\tau) &= \frac{d^2 g(\tau)}{d\tau^2} = \frac{d}{d\tau} (g^{(1)}(\tau)) \\ &= \frac{d}{d\tau} \left[\frac{1}{m!} J^{(1)}(\tau) w^m(\tau) - \frac{m}{m!} x_p^{(1)}(\tau) J(\tau) w^{m-1}(\tau) \right] \\ &= \frac{1}{m!} J^{(2)}(\tau) w^m(\tau) - \frac{m}{m!} J(\tau) x_p^{(2)}(\tau) w^{m-1}(\tau) \\ &\quad + \frac{m(m-1)}{m!} J(\tau) x_p^{(1)}(\tau)^2 w^{m-2}(\tau) \\ &\quad - 2x_p^{(1)}(\tau) J^{(1)}(\tau) \frac{m}{m!} w^{m-1}(\tau), \end{aligned} \quad (92)$$

and it trivially follows, for the higher-order time-derivative

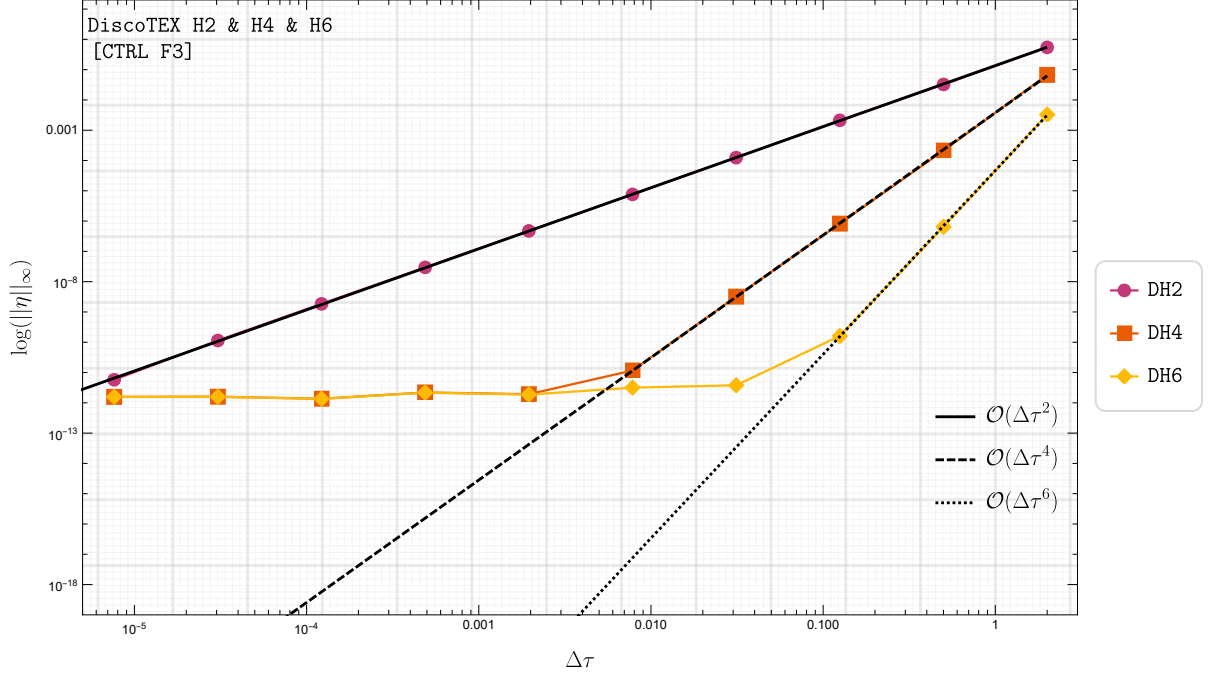


Figure 5: Numerical error associated with computation of the numerical weak-form solution $\Psi(\tau, \sigma_f)$ against the exact solution in equation (4) with both the discontinuous Hermite integrator of order-2, order-4 and order-6, respectively DH2, DH4, DH6. As expected, we observe in lines DH2, DH4, DH6 that the DiscoTEX algorithm converges to its expected orders respectively.

Δ_{Π} corrections, the jumps used are now \mathbb{J}_m as demonstrated in equations ((88), (89)). In the Appendix A.3 we further give the high-order time-derivatives of the g vector needed as the order of the algorithm is further increased in equations ((A.17), (A.21), (A.25)). Here, and unlike in [1], we give the corrections without the diagonalisation, and, duly, the dot product has also been removed. As stressed in that work, as long as the operations are handled with care there will be no need to diagonalise these quantities. As long as we ensure: 1) the derivatives are always acting on the governing evolution field - from the left side; and, 2) if no differential operators are acting on the field variables on $\mathbf{L}_{1/2}$ - like for example the last terms in both equations (60) and (61) - we multiply these terms by the identity matrix, for example, $\varrho(\sigma)$ in equation (60) would be coded as $\varrho(\sigma_i) \times \mathbf{I}$.

DiscoTEX H6's numerical algorithm is thus succinctly

$$\begin{aligned} \mathbf{U}_{n+1} = & \mathbf{U}_n + \mathbf{HFH6} \cdot \left[\mathbf{A} \cdot \left[\mathbf{TEXH6} \cdot \mathbf{U}_n + \frac{\Delta\tau}{10} (\mathbf{s}_n - \mathbf{s}_{n+1}) \right. \right. \\ & + \frac{\Delta\tau^2}{120} \left((\mathbf{s}_n^{(1)} - \mathbf{s}_{n+1}^{(1)}) + \mathbf{L} \cdot (\mathbf{s}_n^{(1)} - \mathbf{s}_{n+1}^{(1)}) \right) \\ & + \frac{\Delta\tau}{2} (\mathbf{s}_n + \mathbf{s}_{n+1}) + \frac{\Delta\tau^2}{10} (\mathbf{s}_n^{(1)} - \mathbf{s}_{n+1}^{(1)}) + \frac{\Delta\tau^3}{120} (\mathbf{s}_n^{(2)} + \mathbf{s}_{n+1}^{(2)}) \\ & \left. \left. + \Upsilon + \mathbf{J}_{H6}(\Delta\tau_x, \Delta\tau) \Xi \right], \end{aligned} \quad (93)$$

where,

$$\mathbf{TEXH6} = \left[\mathbf{I} + \frac{\mathbf{A} \cdot \mathbf{A}}{60} \right]. \quad (94)$$

The higher-order DiscoTEX H8-H12 numerical algorithms can be found in Appendix A.3 through equations ((A.13)-(A.22)). It is left to specify the jumps associated with the implementation of the higher-order time-integration scheme as described in Section 2.3 highlighted in the algorithm by the term $\mathbf{J}_{H6}(\Delta\tau_x, \Delta\tau)$. We need 6 jumps for each of the differential operations in the evolution operators ((60), (61)), i.e.

$$\begin{aligned} \mathbf{J}_j(\tau) &= \left(\mathbb{J} \mathbb{J}_j(\tau) \right) = \\ &= \left(\mathbb{J}_0(\tau), \mathbb{K}_0(\tau), \mathbb{L}_0(\tau), \mathbb{M}_0(\tau), \mathbb{N}_0(\tau), \mathbb{O}_0(\tau) \right) \Big|_{\tau \rightarrow \frac{\sigma_p(\tau)}{v}}. \end{aligned} \quad (95)$$

We refer the reader to Appendix A.4 where the explicit expressions for $\mathbf{J}_0(\tau)$ to $\mathbf{J}_5(\tau)$ are given through equations ((A.26)-(A.59)). Additionally for higher-order DiscoTEX's implementations the following jumps are necessary: - DiscoTEX H8's will require up to $\mathbf{J}_7(\tau)$ jumps; - DiscoTEX H10's will require up to $\mathbf{J}_9(\tau)$ jumps, and finally DiscoTEX H12's will require up to $\mathbf{J}_{11}(\tau)$ jumps.

3.2. DiscoTEX at higher-orders: Numerics discussion

In this work, the focus is on demonstrating the machinery necessary for implementing the DiscoTEX algorithm at higher orders of numerical convergence and how the performance compares. In Figures 2 and 3 the behaviour is the same as for DiscoTEX H4's Figures 8 and 9 [1], as expected. We ran our simulations in the same set-up as in the companion paper described in Section 3.4.3, that is the algorithm spans a temporal

Algorithm	η	Wall-clock times, s	[# CTRL Factors]
DiscoTEX H2	5.5×10^{-6}	10.8018268	3
DiscoTEX H4	7.7×10^{-11}	11.1215158	3
DiscoTEX H6	7.2×10^{-11}	42.847469	3
DiscoTEX H8	7.2×10^{-9}	147.7311478	3
DiscoTEX H10	7.2×10^{-11}	517.8653133	3
DiscoTEX H12	7.2×10^{-11}	1570.6355016	3

Table 2: Comparison between DiscoTEX H2-H12. As hinted by Table 8 of reference [1] increasing the order of integration has not resulted in a significant accuracy improvement for a given time step that would justify the extra computational cost. DiscoTEX H4 offers the best compromise with accuracy and minimal simulation running time with the current numerical framework.

domain of $\tau \in [-1.52, 4.50]$ and a spatial domain of $\sigma = [0, 1]$, where, as expected from the minimal gauge implementation future null infinity \mathcal{S}^+ is mapped to $\sigma = 0$ and the horizon to $\sigma = 1$. The relative error is computed as

$$\eta = \left| 1 - \frac{\Psi_{\text{Numerical}}}{\Psi_{\text{Exact}}} \right|. \quad (96)$$

As reviewed in Section 2 three numerical optimisation control factors need to be studied to ensure optimal implementation of the DiscoTEX algorithm: [CTRL F1] - number of N nodes; [CTRL F2] - number of J jumps and [CTRL F3] - timestep size. Following up from Section 2.3, and to verify whether the algorithm has been implemented correctly, we determine [CTRL F3] and check numerical convergence order is as expected for the given algorithms under study. In Figure 5 there are no surprises and we observe DiscoTEX H2, H4 & H6 converge to their respective orders.

We then assessed [CTRL F1] and [CTRL F2] and determined $N=45$ and $J=19$ to result in an optimal implementation of DiscoTEX H6. Informed by Figure 3, and to ensure fairness in the comparison provided between the different order algorithmic implementations, we select for the numerical simulations the same timestep used in [1] i.e. $\Delta\tau = 0.00666667$. For the assessment of [CTRL F1], 15 jumps were used whereas the numerical tests for determining [CTRL F2] were computed with $N+1=45$ Chebyshev-Gauss-Lobatto collocation nodes. From Figure 4 we can see that the results for the higher-order algorithm closely follow the numerical convergence pattern observed for DiscoTEX H4 without any substantial improvements. To further complement our results we investigate the computational times for all 12 orders of the DiscoTEX algorithm. From Table 2 it is very clear that, for the same numerical control factors, after the sixth-order algorithm the accuracy stagnates while the computational time significantly increases with increasing order of the time-stepper. Compared with Table 8 of the companion paper [1], which computed the simulations for a much longer time i.e. up to $\tau = 10,000$ amounting to half a million timesteps, the computational times are approximately as long as those observed here which only computes about 903 timesteps. The reason for this significant difference is because of the extra time jumps added by the fact our trajectory is time-dependent and hence one needs to account for the jumps in the time direction, unlike the case studied in that section which probed circular orbits i.e. at a fixed particle position of $\sigma = 0.25$, for

example.

We finally note in this paper, that, unlike in the companion paper [1], we don't explicitly show any checks to assess whether the algorithm is capable of giving the solution at either limit of the point-particle position. The reason for this "omission" is that it is a trivial calculation and the procedure is exactly as described in the first paper. In assessing the numerical optimisation [CTRL F1 & F2] we also included the result for the interpolation at the particle value, this is demonstrated in Figure 4.

4. Conclusion

This paper extends the work presented in ref. [1] to higher orders of numerical convergence. The main conclusion of this work is the significant increase in the computational time and accuracy stagnation as we increase past 6th-order. In this work, we give all the necessary machinery required to implement DiscoTEX including all the time jumps that are to be expected from any point-particle trajectory that has a time dependence. We observed that this caused a significant increase in the total numerical simulation running time for a (much) shorter time interval.

For cases where time-dependent point-particle trajectories are unavoidable, such as when modelling highly eccentric EMRIs, higher-order versions of the algorithm should be avoided, especially if conservative self-force computations are to be computed [1, 7, 6]. However, naturally as expected, and it is observed in Figures 1 and 5, higher-order implementations tend to reach higher accuracies faster for longer timesteps. This faster convergence could be very useful for other astrophysical modelling scenarios including the modelling of extremely asymmetric binaries such as XMRIIs. On top of not requiring any higher-order corrections to the self-force, some XMRIIs, depending on the compact object companion, may also more likely be prescribing a circular orbit as they (very) slowly inspiral towards the supermassive black hole [15, 16, 17, 18, 19]. Another area where it may be very useful to use the discontinuous or (smooth!) IMTEX Hermite time-stepper could be black-hole spectroscopy. These applications are left for future work and are to be compared with different numerical algorithms.

Acknowledgements

I would like to thank my PhD supervisors Professors Pau Figueras and Juan Valiente Kroon for their encouragement and guidance in the completion of this work. Finally, it is a pleasure to thank Subrahmanyan Chandrasekhar, whose intelligence and work ethic have been a source of motivation and (inspiration) in the last years of my PhD [20, 8].

Appendix A. Complementary work for the development of the `DiscoTeX` numerical algorithm at higher-orders of numerical convergence

Appendix A.1. Higher-order discontinuous time-integration schemes

As a necessary complement to Section 2.3 the following discontinuous time-integration rules from orders 2nd to 12th are explicitly given below:

$$f(t)_{\text{DH2}} = \frac{\Delta t}{2} \left(f(t_n) + f(t_{n+1}) \right) + \mathbf{J}_{\text{H2}}(\Delta t_{\times}, \Delta t), \quad (\text{A.1})$$

$$f(t)_{\text{DH4}} = \frac{\Delta t}{2} \left(f(t_n) + f(t_{n+1}) \right) + \frac{\Delta t^2}{12} \left(\dot{f}(t_n) - \dot{f}(t_{n+1}) \right) + \mathbf{J}_{\text{H4}}(\Delta t_{\times}, \Delta t), \quad (\text{A.2})$$

$$f(t)_{\text{DH8}} = \frac{\Delta t}{2} \left(f(t_n) + f(t_{n+1}) \right) + \frac{3}{28} \Delta t^2 \left(\dot{f}(t_n) - \dot{f}(t_{n+1}) \right) + \frac{\Delta t^3}{84} \left(\ddot{f}(t_n) + \ddot{f}(t_{n+1}) \right) + \frac{\Delta t^4}{1680} \left(\frac{d^3 f(t_n)}{dt^3} - \frac{d^3 f(t_{n+1})}{dt^3} \right) + \mathbf{J}_{\text{H8}}(\Delta t_{\times}, \Delta t), \quad (\text{A.3})$$

$$f(t)_{\text{NDH6}} = \frac{\Delta t}{2} \left(f(t_v) + f(t_{v+1}) \right) + \frac{\Delta t^2}{10} \left(\dot{f}(t_v) - \dot{f}(t_{v+1}) \right) + \frac{\Delta t^3}{120} \left(\ddot{f}(t_v) + \ddot{f}(t_{v+1}) \right) + \mathbf{J}_{\text{H6}}(\Delta t_{\times}, \Delta t), \quad (\text{A.4})$$

where $\mathbf{J}_{\text{H6}}(\Delta t_{\times}, \Delta t)$ is given by

$$\begin{aligned} \mathbf{J}_{\text{H6}}(\Delta t_{\times}, \Delta t) = & \frac{1}{2} (\Delta t - 2\Delta t_{\times}) \mathbf{J}_0 + \frac{1}{10} (\Delta t^2 - 5\Delta t \Delta t_{\times} + 5\Delta t_{\times}^2) \mathbf{J}_1 + \\ & \frac{1}{120} (\Delta t - 2\Delta t_{\times}) (\Delta t^2 - 10\Delta t \Delta t_{\times} + 10\Delta t_{\times}^2) \mathbf{J}_2 - \\ & \frac{1}{120} (\Delta t - \Delta t_{\times}) \Delta t_{\times} (\Delta t^2 - 5\Delta t \Delta t_{\times} + 5\Delta t_{\times}^2) \mathbf{J}_3 + \\ & \frac{1}{240} (\Delta t - 2\Delta t_{\times}) (\Delta t - \Delta t_{\times})^2 \Delta t_{\times}^2 \mathbf{J}_4 - \\ & \frac{1}{720} (\Delta t - \Delta t_{\times})^3 \Delta t_{\times}^3 \mathbf{J}_5. \end{aligned} \quad (\text{A.5})$$

$$\begin{aligned} f(t)_{\text{DH10}} = & \frac{\Delta t}{2} \left(f(t_n) + f(t_{n+1}) \right) + \frac{\Delta t^2}{9} \left(\dot{f}(t_n) - \dot{f}(t_{n+1}) \right) \\ & + \frac{\Delta t^3}{72} \left(\ddot{f}(t_n) + \ddot{f}(t_{n+1}) \right) + \frac{\Delta t^4}{1008} \left(\frac{d^3 f(t_n)}{dt^3} - \frac{d^3 f(t_{n+1})}{dt^3} \right) \\ & + \frac{\Delta t^5}{30240} \left(\frac{d^4 f(t_n)}{dt^4} + \frac{d^4 f(t_{n+1})}{dt^4} \right) \\ & + \mathbf{J}_{\text{H10}}(\Delta t_{\times}, \Delta t), \end{aligned} \quad (\text{A.6})$$

where $\mathbf{J}_{\text{H2-H12}}(\Delta t_{\times}, \Delta t)$ are given respectively as,

$$\mathbf{J}_{\text{H2}}(\Delta t_{\times}, \Delta t) = \frac{1}{2} (\Delta t - 2\Delta t_{\times}) \mathbf{J}_0 + \frac{\Delta t_{\times}}{2} (\Delta t_{\times} - \Delta t) \mathbf{J}_1, \quad (\text{A.7})$$

$$\begin{aligned} \mathbf{J}_{\text{H4}}(\Delta t_{\times}, \Delta t) = & \frac{1}{2} (\Delta t - 2\Delta t_{\times}) \mathbf{J}_0 + \frac{\Delta t_{\times}^2}{12} (\Delta t^2 - 6\Delta t \Delta t_{\times} + 6\Delta t_{\times}^2) \mathbf{J}_1 \\ & - \frac{1}{12} \Delta t_{\times} (\Delta t^2 - 3\Delta t \Delta t_{\times} + 2\Delta t_{\times}^2) \mathbf{J}_2 + \frac{1}{24} \Delta t_{\times}^2 (\Delta t - \Delta t_{\times}) \mathbf{J}_3 \end{aligned} \quad (\text{A.8})$$

$$\begin{aligned} \mathbf{J}_{\text{H8}}(\Delta t_{\times}, \Delta t) = & \frac{1}{2} (\Delta t - 2\Delta t_{\times}) \mathbf{J}_0 + \frac{1}{28} (3\Delta t^2 - 14\Delta t \Delta t_{\times} + 14\Delta t_{\times}^2) \mathbf{J}_1 + \\ & + \frac{1}{84} (\Delta t - 2\Delta t_{\times}) (\Delta t^2 - 7\Delta t \Delta t_{\times} + 7\Delta t_{\times}^2) \mathbf{J}_2 \\ & + \frac{1}{1680} (\Delta t^4 - 20\Delta t^3 \Delta t_{\times} + 90\Delta t^2 \Delta t_{\times}^2 - 140\Delta t \Delta t_{\times}^3 + 70\Delta t_{\times}^4) \mathbf{J}_3 \\ & - \frac{1}{1680} (\Delta t - 2\Delta t_{\times}) (\Delta t - \Delta t_{\times}) \Delta t_{\times} (\Delta t^2 - 7\Delta t \Delta t_{\times} + 7\Delta t_{\times}^2) \mathbf{J}_4 \\ & + \frac{1}{10080} (\Delta t - \Delta t_{\times})^2 \Delta t_{\times}^2 (3\Delta t^2 - 14\Delta t \Delta t_{\times} + 14\Delta t_{\times}^2) \mathbf{J}_5 \\ & - \frac{1}{10080} (\Delta t - 2\Delta t_{\times}) (\Delta t - \Delta t_{\times})^3 \Delta t_{\times}^3 \mathbf{J}_6 + \frac{1}{40320} (\Delta t - \Delta t_{\times})^4 \Delta t_{\times}^4 \mathbf{J}_7, \end{aligned} \quad (\text{A.9})$$

$$\begin{aligned} \mathbf{J}_{\text{H10}}(\Delta t_{\times}, \Delta t) = & \frac{1}{2} (\Delta t - 2\Delta t_{\times}) \mathbf{J}_0 + \frac{1}{18} (\Delta t - 3\Delta t_{\times}) (2\Delta t - 3\Delta t_{\times}) \\ & + \frac{1}{72} (\Delta t - 2\Delta t_{\times}) (\Delta t^2 - 6\Delta t \Delta t_{\times} + 6\Delta t_{\times}^2) \mathbf{J}_2 \\ & + \frac{1}{1008} (\Delta t^4 - 14\Delta t^3 \Delta t_{\times} + 56\Delta t^2 \Delta t_{\times}^2 - 84\Delta t \Delta t_{\times}^3 + 42\Delta t_{\times}^4) \mathbf{J}_3 \\ & - \frac{1}{30240} (\Delta t - 2\Delta t_{\times}) (\Delta t^4 - 28\Delta t^3 \Delta t_{\times} + 154\Delta t^2 \Delta t_{\times}^2 - 252\Delta t \Delta t_{\times}^3 + 126\Delta t_{\times}^4) \mathbf{J}_4 \\ & + \frac{1}{30240} (\Delta t - \Delta t_{\times}) \Delta t_{\times} (\Delta t^4 - 14\Delta t^3 \Delta t_{\times} + 56\Delta t^2 \Delta t_{\times}^2 - 84\Delta t \Delta t_{\times}^3 + 42\Delta t_{\times}^4) \mathbf{J}_5 \\ & + \frac{1}{60480} (\Delta t - 2\Delta t_{\times}) (\Delta t - \Delta t_{\times})^2 \Delta t_{\times}^2 (\Delta t^2 - 6\Delta t \Delta t_{\times} + 6\Delta t_{\times}^2) \mathbf{J}_6 \\ & - \frac{1}{362880} (\Delta t - 3\Delta t_{\times}) (2\Delta t - 3\Delta t_{\times}) (\Delta t - \Delta t_{\times})^3 \Delta t_{\times}^3 \mathbf{J}_7 \\ & + \frac{1}{725760} (\Delta t - 2\Delta t_{\times}) (\Delta t - \Delta t_{\times})^4 \Delta t_{\times}^4 \mathbf{J}_8 - \frac{1}{3628800} (\Delta t - \Delta t_{\times})^5 \Delta t_{\times}^5 \mathbf{J}_9, \end{aligned} \quad (\text{A.10})$$

Appendix A.2. Supplementary material to the spatial discontinuous discretization

As showed in [1] for the equation in (59) we have the following initialising jumps,

$$J_0 = \bar{\gamma}^2 \frac{\Delta_c(\xi_p)}{|\Delta_c(\xi_p)|^3} F(\tau_c) \quad (\text{A.11})$$

$$J_1 = \bar{\gamma}^2 \left[\frac{\Delta'_c(\xi_p)}{|\Delta_c(\xi_p)|^3} F(\tau_c) - \frac{\Delta_c(\xi_p)}{|\Delta_c(\xi_p)|^3} \frac{\partial F(\tau_c)}{\partial t} \frac{\partial t}{\partial \xi_p} + \frac{G(\tau_c)}{\Delta_c(\xi_p)} + \left(\dot{\xi}_p \Gamma(\xi_p) + \dot{\xi}_p^2 \Gamma'(\xi_p) - \dot{\xi}_p \varepsilon'(\xi_p) + \varrho'(\xi_p) \chi'(\xi_p) - \iota(\xi_p) \right) J_0 + \left(2\dot{\xi}_p \Gamma(\xi_p) - \varepsilon(\xi_p) \right) J_0 \right]. \quad (\text{A.12})$$

where $\tau_c = t(\tau, \sigma_p(\tau))$, $\xi_p = x(\sigma_p(\tau))$.

Appendix A.3. Higher-order DiscoTEX algorithm

For completion, we include all the DiscoTEX algorithms from 2th- to 12th- order of time-integration.

The simplest algorithm is DiscoTEX H2 given as,

$$\mathbf{U}_{n+1} = \mathbf{U}_n + \mathbf{HFH2} \cdot \left[\mathbf{A} \cdot \mathbf{U}_n + \frac{\Delta\tau}{2} (\mathbf{s}_n + \mathbf{s}_{n+1}) + \Upsilon + \mathbf{J}_{H2}(\Delta\tau_x, \Delta\tau) \Xi \right]. \quad (\text{A.13})$$

DiscoTEX H8 is given by,

$$\begin{aligned} \mathbf{U}_{n+1} = \mathbf{U}_n + \mathbf{HFH8} \cdot \left[\mathbf{A} \cdot \left[\mathbf{TEXH8} \cdot \mathbf{U}_n + \frac{3\Delta\tau}{28} (\mathbf{s}_n - \mathbf{s}_{n+1}) \right] \right. \\ + \frac{\Delta\tau^2}{84} \left((\mathbf{s}_n^{(1)} + \mathbf{s}_{n+1}^{(1)}) + \mathbf{L} \cdot (\mathbf{s}_n + \mathbf{s}_{n+1}) \right) + \\ + \frac{\Delta\tau^3}{1680} \left((\mathbf{s}_n^{(2)} - \mathbf{s}_{n+1}^{(2)}) + \mathbf{L} \cdot (\mathbf{s}_n^{(1)} - \mathbf{s}_{n+1}^{(1)}) + \mathbf{L} \cdot \mathbf{L} \cdot (\mathbf{s}_n - \mathbf{s}_{n+1}) \right) \\ + \frac{\Delta\tau}{2} (\mathbf{s}_n + \mathbf{s}_{n+1}) + \frac{3\Delta\tau^2}{28} (\mathbf{s}_n^{(1)} - \mathbf{s}_{n+1}^{(1)}) + \frac{\Delta\tau^3}{84} (\mathbf{s}_n^{(2)} + \mathbf{s}_{n+1}^{(2)}) \\ \left. + \frac{\Delta\tau^3}{1680} (\mathbf{s}_n^{(3)} - \mathbf{s}_{n+1}^{(3)}) + \Upsilon + \mathbf{J}_{H8}(\Delta\tau_x, \Delta\tau) \Xi \right]. \quad (\text{A.14}) \end{aligned}$$

where,

$$\mathbf{TEXH8} = \left[\mathbf{I} + \frac{\mathbf{A} \cdot \mathbf{A}}{42} \right], \quad (\text{A.15})$$

and we have used the replacement,

$$\begin{aligned} \mathbf{U}^{(3)} = \frac{d}{d\tau} \mathbf{U}^{(2)} = \\ = \mathbf{L} \cdot \mathbf{L} \cdot \mathbf{L} \cdot \mathbf{U} + \mathbf{L} \cdot \mathbf{L} \cdot \mathbf{S} + \mathbf{L} \cdot \mathbf{S}^{(1)} + \mathbf{S}^{(2)}. \quad (\text{A.16}) \end{aligned}$$

It will be further necessary to compute,

$$\begin{aligned} g^{(3)}(\tau) = \frac{d^3 g(\tau)}{d\tau^3} = \frac{d}{d\tau} (g^{(2)}(\tau)) \\ = \frac{1}{m!} J^{(3)} w^m - \frac{m}{m!} [3J^{(2)} x_p^{(1)} + 3J^{(1)} x_p^{(2)} + J x_p^{(3)}] w^{m-1} \\ + \frac{m(m-1)}{m!} [3(x_p^{(1)})^2 J^{(1)} + 3x_p^{(1)} x_p^{(2)}] w^{m-2} \\ - \frac{m(m-1)(m-2)}{m!} (x_p^{(1)})^3 J w^{m-3}. \quad (\text{A.17}) \end{aligned}$$

Similarly DiscoTEX H10 is given by,

$$\begin{aligned} \mathbf{U}_{n+1} = \mathbf{U}_n + \mathbf{HFH10} \cdot \left[\mathbf{A} \cdot \left[\mathbf{TEXH10} \cdot \mathbf{U}_n + \frac{\Delta\tau}{9} (\mathbf{s}_n - \mathbf{s}_{n+1}) \right] \right. \\ + \frac{\Delta\tau^2}{72} \left((\mathbf{s}_n^{(1)} + \mathbf{s}_{n+1}^{(1)}) + \mathbf{L} \cdot (\mathbf{s}_n + \mathbf{s}_{n+1}) \right) + \\ + \frac{\Delta\tau^3}{1008} \left((\mathbf{s}_n^{(2)} - \mathbf{s}_{n+1}^{(2)}) + \mathbf{L} \cdot (\mathbf{s}_n^{(1)} - \mathbf{s}_{n+1}^{(1)}) + \mathbf{L} \cdot \mathbf{L} \cdot (\mathbf{s}_n - \mathbf{s}_{n+1}) \right) \\ + \frac{\Delta\tau^4}{30240} \left((\mathbf{s}_n^{(3)} + \mathbf{s}_{n+1}^{(3)}) + \mathbf{L} \cdot (\mathbf{s}_n^{(2)} + \mathbf{s}_{n+1}^{(2)}) + \right. \\ \left. + \mathbf{L} \cdot \mathbf{L} \cdot (\mathbf{s}_n^{(1)} + \mathbf{s}_{n+1}^{(1)}) + \mathbf{L} \cdot \mathbf{L} \cdot \mathbf{L} \cdot (\mathbf{s}_n + \mathbf{s}_{n+1}) \right) \\ + \frac{\Delta\tau}{2} (\mathbf{s}_n + \mathbf{s}_{n+1}) + \frac{\Delta\tau^2}{9} (\mathbf{s}_n^{(1)} - \mathbf{s}_{n+1}^{(1)}) + \frac{\Delta\tau^3}{72} (\mathbf{s}_n^{(2)} + \mathbf{s}_{n+1}^{(2)}) \\ + \frac{\Delta\tau^4}{1008} (\mathbf{s}_n^{(3)} - \mathbf{s}_{n+1}^{(3)}) + \frac{\Delta\tau^5}{30240} (\mathbf{s}_n^{(4)} + \mathbf{s}_{n+1}^{(4)}) \\ \left. + \Upsilon + \mathbf{J}_{H10}(\Delta\tau_x, \Delta\tau) \Xi \right]. \quad (\text{A.18}) \end{aligned}$$

where,

$$\mathbf{TEXH10} = \left[\mathbf{I} + \mathbf{A} \cdot \mathbf{A} \cdot \left(\frac{\mathbf{I}}{36} + \frac{\mathbf{A} \cdot \mathbf{A}}{1520} \right) \right], \quad (\text{A.19})$$

with the replacement

$$\begin{aligned} \mathbf{U}^{(4)} = \frac{d}{d\tau} \mathbf{U}^{(3)} = \\ = \mathbf{L} \cdot \mathbf{L} \cdot \mathbf{L} \cdot \mathbf{L} \cdot \mathbf{U} + \mathbf{L} \cdot \mathbf{L} \cdot \mathbf{L} \cdot \mathbf{S} + \mathbf{L} \cdot \mathbf{L} \cdot \mathbf{S}^{(1)} \\ + \mathbf{L} \cdot \mathbf{S}^{(2)} + \mathbf{S}^{(3)}. \quad (\text{A.20}) \end{aligned}$$

In addition to equation (A.17), the higher-order $g^{(4)}(\tau)$ will also be necessary,

$$\begin{aligned} g^{(4)}(\tau) = \frac{d^4 g(\tau)}{d\tau^4} = \frac{d}{d\tau} (g^{(3)}(\tau)) \\ = \frac{1}{m!} J^{(4)}(\tau) w^m(\tau) \\ - \frac{m}{m!} [x_p^{(4)} J + 4x_p^{(3)} J^{(1)} + 6x_p^{(2)} J^{(2)} + 4x_p^{(1)} J^{(3)}] w^{m-1} \\ + \frac{m(m-1)}{m!} [4x_p^{(1)} x_p^{(3)} J + 12x_p^{(1)} x_p^{(2)} J^{(1)} \\ + 6(x_p^{(1)})^2 J^{(1)} + 3(x_p^{(2)})^2 J] w^{m-2} \\ - \frac{m(m-1)(m-2)}{m!} [6(x_p^{(1)})^2 x_p^{(2)} J + 4(x_p^{(1)})^3 J^{(1)}] w^{m-3} \\ + \frac{m(m-1)(m-2)(m-3)}{m!} (x_p^{(1)})^4 J w^{m-4}. \quad (\text{A.21}) \end{aligned}$$

Finally DiscoTEX H12 is given by,

$$\begin{aligned}
\mathbf{U}_{n+1} = & \mathbf{U}_n + \mathbf{HFH12} \cdot \left[\mathbf{A} \cdot \left[\mathbf{TEXH12} \cdot \mathbf{U}_n + \frac{5\Delta\tau}{44} (\mathbf{s}_n + \mathbf{s}_{n+1}) \right. \right. \\
& + \frac{\Delta\tau^2}{66} \left((\mathbf{s}_n^{(1)} + \mathbf{s}_{n+1}^{(1)}) + \mathbf{L} \cdot (\mathbf{s}_n + \mathbf{s}_{n+1}) \right) + \\
& + \frac{\Delta\tau^3}{792} \left((\mathbf{s}_n^{(2)} - \mathbf{s}_{n+1}^{(2)}) + \mathbf{L} \cdot (\mathbf{s}_n^{(1)} - \mathbf{s}_{n+1}^{(1)}) + \mathbf{L} \cdot \mathbf{L} \cdot (\mathbf{s}_n - \mathbf{s}_{n+1}) \right) \\
& + \frac{\Delta\tau^4}{15840} \left((\mathbf{s}_n^{(3)} + \mathbf{s}_{n+1}^{(3)}) + \mathbf{L} \cdot (\mathbf{s}_n^{(2)} + \mathbf{s}_{n+1}^{(2)}) + \mathbf{L} \cdot \mathbf{L} \cdot (\mathbf{s}_n^{(1)} + \mathbf{s}_{n+1}^{(1)}) \right. \\
& \left. + \mathbf{L} \cdot \mathbf{L} \cdot \mathbf{L} \cdot (\mathbf{s}_n + \mathbf{s}_{n+1}) \right) \\
& + \frac{\Delta\tau^5}{665280} \left((\mathbf{s}_n^{(4)} - \mathbf{s}_{n+1}^{(4)}) + \mathbf{L} \cdot (\mathbf{s}_n^{(3)} - \mathbf{s}_{n+1}^{(3)}) \right. \\
& + \mathbf{L} \cdot \mathbf{L} \cdot (\mathbf{s}_n^{(2)} - \mathbf{s}_{n+1}^{(2)}) + \mathbf{L} \cdot \mathbf{L} \cdot \mathbf{L} \cdot (\mathbf{s}_n^{(1)} - \mathbf{s}_{n+1}^{(1)}) \\
& \left. + \mathbf{L} \cdot \mathbf{L} \cdot \mathbf{L} \cdot \mathbf{L} \cdot (\mathbf{s}_n - \mathbf{s}_{n+1}) \right) \\
& + \frac{\Delta\tau}{2} (\mathbf{s}_n - \mathbf{s}_{n+1}) + \frac{5\Delta\tau^2}{44} (\mathbf{s}_n^{(1)} - \mathbf{s}_{n+1}^{(1)}) + \frac{\Delta\tau^3}{66} (\mathbf{s}_n^{(2)} - \mathbf{s}_{n+1}^{(2)}) \\
& + \frac{\Delta\tau^4}{792} (\mathbf{s}_n^{(3)} - \mathbf{s}_{n+1}^{(3)}) + \frac{\Delta\tau^5}{15840} (\mathbf{s}_n^{(4)} - \mathbf{s}_{n+1}^{(4)}) \\
& \left. + \frac{\Delta\tau^6}{665280} (\mathbf{s}_n^{(5)} - \mathbf{s}_{n+1}^{(5)}) + \Upsilon + \mathbf{J}_{H12}(\Delta\tau_x, \Delta\tau) \Xi \right]. \quad (\text{A.22})
\end{aligned}$$

where,

$$\mathbf{TEXH12} = \left[\mathbf{I} + \mathbf{A} \cdot \mathbf{A} \cdot \left(\frac{\mathbf{I}}{33} + \frac{\mathbf{A} \cdot \mathbf{A}}{7920} \right) \right], \quad (\text{A.23})$$

with the replacement,

$$\begin{aligned}
\mathbf{U}^{(5)} = & \frac{d}{d\tau} \mathbf{U}^{(4)} = \\
= & \mathbf{L} \cdot \mathbf{L} \cdot \mathbf{L} \cdot \mathbf{L} \cdot \mathbf{L} \cdot \mathbf{U} + \mathbf{L} \cdot \mathbf{L} \cdot \mathbf{L} \cdot \mathbf{L} \cdot \mathbf{S} + \mathbf{L} \cdot \mathbf{L} \cdot \mathbf{L} \cdot \mathbf{S}^{(1)} \\
& + \mathbf{L} \cdot \mathbf{L} \cdot \mathbf{S}^{(2)} + \mathbf{L} \cdot \mathbf{S}^{(3)} + \mathbf{S}^{(4)}, \quad (\text{A.24})
\end{aligned}$$

and the additional higher-order $g^{(5)}(\tau)$ vector,

$$\begin{aligned}
g^{(5)}(\tau) = & \frac{d^5 g(\tau)}{d\tau^5} = \frac{d}{d\tau} (g^{(4)}(\tau)) \\
= & \frac{1}{m!} J^{(5)}(\tau) w^m(\tau) \\
& - \frac{m}{m!} \left[J x_p^{(5)} + 5x_p^{(4)} J^{(1)} + 10x_p^{(3)} J^{(2)} + 10x_p^{(2)} J^{(3)} + 5x_p^{(1)} J^{(4)} \right] w^{m-1} \\
& + \frac{m(m-1)}{m!} \left[5x_p^{(1)} x_p^{(4)} J + 10x_p^{(2)} x_p^{(3)} J + 20x_p^{(1)} x_p^{(3)} J^{(1)} \right. \\
& \left. + 15(x_p^{(2)})^2 J^{(1)} + 30x_p^{(1)} x_p^{(2)} J^{(2)} + 10(x_p^{(1)})^2 J^{(3)} \right] w^{m-2} \\
& - \frac{m(m-1)(m-2)}{m!} \left[10(x_p^{(1)})^2 x_p^{(3)} J + 15x_p^{(1)} (x_p^{(2)})^2 J \right. \\
& \left. + 30(x_p^{(1)})^2 x_p^{(2)} J^{(1)} + 10(x_p^{(1)})^3 J^{(2)} \right] w^{m-3} \\
& + \frac{m(m-1)(m-2)(m-3)}{m!} \left[10(x_p^{(1)})^3 x_p^{(2)} J + 5(x_p^{(1)})^4 J^{(1)} \right] w^{m-4} \\
& - \frac{m(m-1)(m-2)(m-3)(m-4)}{m!} (x_p^{(1)})^5 J w^{m-5}. \quad (\text{A.25})
\end{aligned}$$

Appendix A.4. Time jumps for the implementation of DiscoTEX in the (τ, σ) minimal gauge coordinate chart

The time jumps necessary for the implementation $\mathbf{J}_{H2-12}(\Delta t_x, \Delta\tau)$ are explicitly given as:

$$\mathbb{J}_0 = \frac{4}{15} \cos \tau_c + \frac{272}{225} i \sin \tau_c \quad (\text{A.26})$$

$$\mathbb{K}_0 = \frac{4864}{3375} i \cos \tau_c - \frac{128}{225} \sin \tau_c, \quad (\text{A.27})$$

$$\mathbb{L}_0 = -\frac{3136}{3375} \cos \tau_c - \frac{90368}{50625} i \sin \tau_c, \quad (\text{A.28})$$

$$\mathbb{M}_0 = -\frac{1724416}{759375} i \cos \tau_c + \frac{69632}{50625} \sin \tau_c, \quad (\text{A.29})$$

$$\mathbb{N}_0 = \frac{1475584}{759375} \cos \tau_c + \frac{33492992}{11390625} i \sin \tau_c, \quad (\text{A.30})$$

$$\mathbb{O}_0 = \frac{657915904}{170859375} i \cos \tau_c - \frac{30507008}{11390625} \sin \tau_c, \quad (\text{A.31})$$

$$\mathbb{P}_0 = -\frac{622084096}{170859375} \cos \tau_c - \frac{13014990848}{2562890625} i \sin \tau_c, \quad (\text{A.32})$$

$$\mathbb{Q}_0 = -\frac{258579890176}{38443359375} i \cos \tau_c + \frac{12585009152}{2562890625} \sin \tau_c, \quad (\text{A.33})$$

$$\mathbb{R}_0 = \frac{253420109824}{38443359375} \cos \tau_c + \frac{5150958682112}{576650390625} i \sin \tau_c, \quad (\text{A.34})$$

$$\mathbb{S}_0 = \frac{102771504185344}{8649755859375} i \cos \tau_c - \frac{5089041317888}{576650390625} \sin \tau_c, \quad (\text{A.35})$$

$$\mathbb{T}_0 = -\frac{102028495814656}{8649755859375} \cos \tau_c - \frac{2052458050224128}{129746337890625} i \sin \tau_c, \quad (\text{A.36})$$

$$\mathbb{U}_0 = -\frac{41013496602689536}{1946195068359375} i \cos \tau_c + \frac{2043541949775872}{129746337890625} \sin \tau_c, \quad (\text{A.37})$$

As we have done in Section of ref.[1] throughout equations ((145)-(159)) we need to incorporate the differential operators in \mathbf{L} , as defined in Eqs. ((59), (60) - (61)) into the final time jump associated with the $\mathbf{L}_{1,2}$ operators. We thus introduce the following additional higher-order terms,

$$\mathcal{J}_0 = \mathcal{J}_{0,x} + \mathcal{J}_{0,t} + \mathcal{J}_{0,\varepsilon} + \mathcal{J}_{0,\varrho}, \quad (\text{A.38})$$

$$\mathcal{K}_0 = \mathcal{K}_{0,x} + \mathcal{K}_{0,t} + \mathcal{K}_{0,\varepsilon} + \mathcal{K}_{0,\varrho}, \quad (\text{A.39})$$

$$\mathcal{L}_0 = \mathcal{L}_{0,x} + \mathcal{L}_{0,t} + \mathcal{L}_{0,\varepsilon} + \mathcal{L}_{0,\varrho}, \quad (\text{A.40})$$

$$\mathcal{M}_0 = \mathcal{M}_{0,x} + \mathcal{M}_{0,t} + \mathcal{M}_{0,\varepsilon} + \mathcal{M}_{0,\varrho}, \quad (\text{A.41})$$

$$\mathcal{N}_0 = \mathcal{N}_{0,x} + \mathcal{N}_{0,t} + \mathcal{N}_{0,\varepsilon} + \mathcal{N}_{0,\varrho}, \quad (\text{A.42})$$

$$\mathcal{O}_0 = \mathcal{O}_{0,x} + \mathcal{O}_{0,t} + \mathcal{O}_{0,\varepsilon} + \mathcal{O}_{0,\varrho}, \quad (\text{A.43})$$

$$\mathcal{P}_0 = \mathcal{P}_{0,x} + \mathcal{P}_{0,t} + \mathcal{P}_{0,\varepsilon} + \mathcal{P}_{0,\varrho}, \quad (\text{A.44})$$

$$\mathcal{Q}_0 = \mathcal{Q}_{0,x} + \mathcal{Q}_{0,t} + \mathcal{Q}_{0,\varepsilon} + \mathcal{Q}_{0,\varrho}, \quad (\text{A.45})$$

$$\mathcal{R}_0 = \mathcal{R}_{0,x} + \mathcal{R}_{0,t} + \mathcal{R}_{0,\varepsilon} + \mathcal{R}_{0,\varrho}, \quad (\text{A.46})$$

$$\mathcal{S}_0 = \mathcal{S}_{0,x} + \mathcal{S}_{0,t} + \mathcal{S}_{0,\varepsilon} + \mathcal{S}_{0,\varrho}, \quad (\text{A.47})$$

$$\mathcal{T}_0 = \mathcal{T}_{0,x} + \mathcal{T}_{0,t} + \mathcal{T}_{0,\varepsilon} + \mathcal{T}_{0,\varrho}, \quad (\text{A.48})$$

$$\mathcal{U}_0 = \mathcal{U}_{0,x} + \mathcal{U}_{0,t} + \mathcal{U}_{0,\varepsilon} + \mathcal{U}_{0,\varrho}, \quad (\text{A.49})$$

Following ref.[1] we correct the differential operators which contain a coefficient given in terms of the σ coordinate. In short¹, we define,

$$\mathcal{J}(\tau) = \mathcal{J}_{(0,\chi),\bar{m}} + \mathcal{J}_{(0,\iota),\bar{m}} + \mathcal{J}_{(0,\varepsilon),\bar{m}} + \mathcal{J}_{(0,\varrho),\bar{m}}, \quad (\text{A.50})$$

where $\bar{m} = \{\bar{k}, \dots, m - \bar{k}\}$ and \bar{k} is variable depending on the coefficient of the differential operator in question. Each of these terms is given as,

$$\mathcal{J}_{0,\chi} = \sum_{k=0}^{\bar{m}} \binom{\bar{m}}{k} \tilde{\chi}^{(k)}(\xi_p) J_{\bar{m}-k}(\tau), \quad (\text{A.51})$$

$$\mathcal{J}_{0,\iota} = \sum_{k=0}^{\bar{m}} \binom{\bar{m}}{k} \tilde{\iota}^{(k)}(\xi_p) J_{\bar{m}-k}(\tau), \quad (\text{A.52})$$

$$\mathcal{J}_{0,\varepsilon} = \sum_{k=0}^{\bar{m}} \binom{\bar{m}}{k} \tilde{\varepsilon}^{(k)}(\xi_p) J_{\bar{m}-k}(\tau), \quad (\text{A.53})$$

$$\mathcal{J}_{0,\varrho} = \sum_{k=0}^{\bar{m}} \binom{\bar{m}}{k} \tilde{\varrho}^{(k)}(\xi_p) J_{\bar{m}-k}(\tau), \quad (\text{A.54})$$

$$\mathcal{J}_0(\tau) = \mathcal{J}_{0,\chi}|_{\bar{k}=2} + \mathcal{J}_{0,\iota}|_{\bar{k}=1} + \mathcal{J}_{0,\varepsilon}|_{\bar{k}=0} + \mathcal{J}_{0,\varrho}|_{\bar{k}=1}. \quad (\text{A.55})$$

All the remainder higher-order terms are determined in an analogous trivial process which we omit for brevity. Below we give

¹For more details see Appendices A and D of [1].

the final results:

$$\mathcal{J}_0 = \frac{4((225 + 1216i) \cos \tau_c - (480 - 1020i) \sin \tau_c)}{3375}, \quad (\text{A.56})$$

$$\mathcal{K}_0 = \frac{64((-735 + 1140i) \cos \tau_c - (450 - 1412i) \sin \tau_c)}{50625}, \quad (\text{A.57})$$

$$\mathcal{L}_0 = -\frac{64((11025 + 26944i) \cos \tau_c - (16320 - 21180i) \sin \tau_c)}{759375}, \quad (\text{A.58})$$

$$\mathcal{M}_0 = \frac{(22133760 - 25866240i) \cos \tau_c}{11390625} + \frac{(15667200 + 33492992i) \sin \tau_c}{11390625}, \quad (\text{A.59})$$

$$\mathcal{N}_0 = \frac{1024(324225 + 642496i) \cos \tau_c}{170859375} - \frac{1024(446880 - 490620i) \sin \tau_c}{170859375}, \quad (\text{A.60})$$

$$\mathcal{O}_0 = \frac{16384(-569535 + 602340i) \cos \tau_c}{2562890625} - \frac{16384(418950 + 794372i) \sin \tau_c}{2562890625}, \quad (\text{A.61})$$

$$\mathcal{P}_0 = \frac{16384(8543025 + 15782464i) \cos \tau_c}{38443359375} - \frac{16384(11521920 - 11915580i) \sin \tau_c}{38443359375}, \quad (\text{A.62})$$

$$\mathcal{Q}_0 = \frac{(3801301647360 - 3878698352640i) \cos \tau_c}{576650390625} + \frac{(2831627059200 + 5150958682112i) \sin \tau_c}{576650390625}, \quad (\text{A.63})$$

$$\mathcal{R}_0 = \frac{262144(217512225 + 392042176i) \cos \tau_c}{8649755859375} - \frac{262144(291197280 - 294740220i) \sin \tau_c}{8649755859375}, \quad (\text{A.64})$$

$$\mathcal{S}_0 = \frac{4194304(-364882335 + 367539540i) \cos \tau_c}{129746337890625} - \frac{4194304(272997450 + 489344132i) \sin \tau_c}{129746337890625}, \quad (\text{A.65})$$

$$\mathcal{T}_0 = -\frac{4194304(5473235025 + 9778379584i) \cos \tau_c}{1946195068359375} - \frac{4194304(7308275520 - 7340161980i) \sin \tau_c}{1946195068359375}, \quad (\text{A.66})$$

$$\mathcal{U}_0 = \frac{(613597550959656960 - 615202449040343040i) \cos \tau_c}{29192926025390625} + \frac{(459796938699571200 + 819841959232274432i) \sin \tau_c}{29192926025390625}, \quad (\text{A.67})$$

Finally, we note all these equations and others are given before taking the limit as previously explained.

References

- [1] L. J. G. Da Silva, Discotex: Discontinuous collocation and implicit-
turned-explicit (imtex) integration symplectic, symmetric numerical al-
gorithms with higher order jumps for differential equations with nu-
merical black hole perturbation theory applications, arXiv preprint
arXiv:2401.08758 (2024).
- [2] S. E. Field, J. S. Hesthaven, S. R. Lau, Discontinuous galerkin method
for computing gravitational waveforms from extreme mass ratio binaries,
Classical and Quantum Gravity 26 (16) (2009) 165010.
- [3] S. E. Field, J. S. Hesthaven, S. R. Lau, Persistent junk solutions in time-
domain modeling of extreme mass ratio binaries, *Physical Review D*
81 (12) (2010) 124030.
- [4] S. E. Field, S. Gottlieb, G. Khanna, E. McClain, Discontinuous galerkin
method for linear wave equations involving derivatives of the dirac delta
distribution, in: *Spectral and High Order Methods for Partial Differential
Equations ICOSAHOM 2020+ 1: Selected Papers from the ICOSAHOM
Conference, Vienna, Austria, July 12-16, 2021, Springer, 2022, pp. 307–
321.*
- [5] S. E. Field, Exact solutions to distributionally sourced wave equations ex-
tending [2] Appendix B to higher order deltas, unpublished work (2023).
- [6] N. Afshordi, S. Akçay, P. A. Seoane, A. Antonelli, J. C. Aurrekoetxea,
L. Barack, E. Barausse, R. Benkel, L. Bernard, S. Bernuzzi, et al., Wave-
form modelling for the laser interferometer space antenna, arXiv preprint
arXiv:2311.01300 (2023).
- [7] L. J. Gomes Da Silva, R. P. Macedo, J. E. Thompson, J. A. V. Kroon,
L. Durkan, O. Long, Hyperboloidal discontinuous time-symmetric nu-
merical algorithm with higher order jumps for gravitational self-force
computations in the time domain, arXiv preprint arXiv:2306.13153
(2023).
- [8] L. J. Gomes Da Silva, Advanced numerical algorithms for EMRIs mod-
elling in the time domain via DiscoTEX and relatives - ground-zero of
the workpackage [E/(X)MRIs@DiscoTEX], PhD thesis, QMUL Univer-
sity, School of Mathematical Sciences, [https://qmro.qmul.ac.uk/
xmlui/handle/123456789/99539](https://qmro.qmul.ac.uk/xmlui/handle/123456789/99539) (2024).
- [9] A. Zenginoğlu, Hyperboloidal foliations and scri-fixing, *Classical and
Quantum Gravity* 25 (14) (2008) 145002.
- [10] A. Zenginoğlu, D. Nunez, S. Husa, Gravitational perturbations of
schwarzschild spacetime at null infinity and the hyperboloidal initial
value problem, *Classical and Quantum Gravity* 26 (3) (2009) 035009.
- [11] M. Ansorg, R. P. Macedo, Spectral decomposition of black-hole perturba-
tions on hyperboloidal slices, *Physical Review D* 93 (12) (2016) 124016.
- [12] J. L. Jaramillo, R. P. Macedo, L. Al Sheikh, Pseudospectrum and black
hole quasinormal mode instability, *Physical Review X* 11 (3) (2021)
031003.
- [13] R. P. Macedo, J. L. Jaramillo, M. Ansorg, Hyperboloidal slicing approach
to quasinormal mode expansions: The reissner-nordström case, *Physical
Review D* 98 (12) (2018) 124005.
- [14] R. P. Macedo, Hyperboloidal framework for the kerr spacetime, *Classical
and Quantum Gravity* 37 (6) (2020) 065019.
- [15] P. Amaro-Seoane, Extremely large mass-ratio inspirals, *Physical Review
D* 99 (12) (2019) 123025.
- [16] E. Gourgoulhon, A. Le Tiec, F. H. Vincent, N. Warburton, Gravitational
waves from bodies orbiting the galactic center black hole and their de-
tectability by lisa, *Astronomy & Astrophysics* 627 (2019) A92.
- [17] S. Barsanti, V. De Luca, A. Maselli, P. Pani, Detecting subsolar-mass pri-
mordial black holes in extreme mass-ratio inspirals with lisa and einstein
telescope, *Physical Review Letters* 128 (11) (2022) 111104.
- [18] V. Vázquez-Aceves, L. Zwick, E. Bortolas, P. R. Capelo,
P. Amaro Seoane, L. Mayer, X. Chen, Revised event rates for ex-
treme and extremely large mass-ratio inspirals, *Monthly Notices of the
Royal Astronomical Society* 510 (2) (2022) 2379–2390.
- [19] V. Vázquez-Aceves, Y. Lin, A. Torres-Orjuela, Sgr a* spin and mass esti-
mates through the detection of an extremely large mass-ratio inspiral, *The
Astrophysical Journal* 952 (2) (2023) 139.
- [20] A. Sekhar, Subrahmanyan Chandrasekhar: A man of stellar
physics and stellar grace, [https://thewire.in/the-sciences/
subrahmanyan-chandrasekhar-a-man-of-stellar-physics-and-stellar-grace](https://thewire.in/the-sciences/subrahmanyan-chandrasekhar-a-man-of-stellar-physics-and-stellar-grace),
accessed: 31/10/2023.